1 **Cep55 overexpression promotes genomic instability and tumorigenesis in mice**

2 Debottam Sinha[1,2], Purba Nag[1,2], Devathri Nanayakkara[1], Pascal H.G. Duijf[3,4], Andrew

3 Burgess[5], Prahlad Raninga[1], Veronique A.J. Smits[6,7,8], Amanda L. Bain[1], Goutham

4 Subramanian[1], Meaghan Wall[9], John. W. Finnie[10], Murugan Kalimutho[1,11*], Kum Kum

5 Khanna[1,11*]

6 [1]QIMR Berghofer Medical Research Institute, 300 Herston Road, Herston, QLD 4006,

7 Australia.

8 [2]School of Environment and Sciences, Griffith University, Nathan, QLD 4111, Australia.

9 [3]University of Queensland Diamantina Institute, The University of Queensland, Translational

10 Research Institute, Brisbane, QLD 4102, Australia.

11 [4]Institute of Health and Biomedical Innovation and School of Biomedical Sciences,

12 Queensland University of Technology, Brisbane, Australia.

13 [5]ANZAC Research Institute, University of Sydney, Sydney, NSW, Australia.

14 [6]Unidad de Investigación, Hospital Universitario de Canarias, Instituto de Tecnologías

15 Biomédicas, Tenerife, Spain.

16 [7]Instituto de Tecnologías Biomédicas, Universidad de La Laguna, Tenerife, Spain.

17 [8]Universidad Fernando Pessoa Canarias, Las Palmas de Gran Canaria, Spain.

18 [9]Victorian Cancer Cytogenetics Service, St. Vincent's Hospital, Fitzroy, Melbourne,
19 Australia.

21 [10]Discipline of Anatomy and Pathology, Adelaide Medical School, University of Adelaide

22 and SA Pathology, Adelaide, Australia.

23 [11]These authors contributed equally

24 *Correspondence: Murugan.Kalimutho@qimrberghofer.edu.au (M.K),

25   KumKum.Khanna@qimrberghofer.edu.au (K.K.K)

26 Running Tittle: Cep55 overexpression drives tumorigenesis in mice.

Abstract

High expression of centrosomal protein CEP55 has been correlated with clinico-pathological parameters across multiple human cancers. Despite significant *in vitro* studies and association of aberrantly overexpressed CEP55 with worse prognosis, its causal role *in vivo* tumorigenesis remains elusive. Here, using a ubiquitously overexpressing transgenic mouse model, we show that *Cep55* overexpression causes spontaneous tumorigenesis and accelerates $Trp53^{+/-}$ induced tumours *in vivo*. At the cellular level, using mouse embryonic fibroblasts (MEFs), we demonstrate that *Cep55* overexpression induces proliferation advantage by modulating multiple cellular signalling networks including the PI3K/AKT pathway. Notably, the *Cep55* overexpressing MEFs demonstrate high level of mitotic chromosomal instability (CIN) due to stabilized microtubules. Interestingly, *Cep55* overexpressing MEFs have a compromised Chk1-dependent S-phase checkpoint, causing increased replication speed and DNA damage, resulting in a prolonged aberrant mitotic division. Importantly, this phenotype was rescued by pharmacological inhibition of Pi3k/Akt or expression of mutant Chk1 (S280A), that is insensitive to regulation by active AKT, in *Cep55* overexpressing cell. Collectively, our data demonstrates causative effects of deregulated Cep55 on genome stability and tumorigenesis which have potential implications for tumour initiation and therapy.

1 Introduction

2   Genomic instability (GI) is a hallmark of almost all human cancers. Chromosomal

3 instability (CIN) is a major form of GI, which refers to the acquisition of abnormal

4 chromosome numbers or structures[1]. CIN in cancers primarily occur due to defective mitosis,

5 including biased chromosome segregation and failure to undergo cytokinesis. Both mitotic

6 checkpoint weakness and/or activation can also lead to CIN, exploring its genetic basis has

7 the potential to uncover major mechanism of GI in cancers and therapeutic modality[2].

8   CEP55 is a coiled-coil centrosomal protein which plays a critical role in cytokinetic

9 abscission during mitotic exit[3]. CEP55 is a cancer testis antigen whose expression is

10 restricted to male germ cells in adult animals, however it is re-expressed in a wide variety of

11 cancers[4]. Over the last decade, multiple studies have shown variable associations of

12 overexpressed CEP55 with poor prognosis in human cancers (reviewed by Jeffery *et al*. [4]).

13 On the other hand, loss-of-function mutations in *CEP55* cause Meckel-like and MARCH

14 syndromes[5-8]. Notably, increased CEP55 expression correlates with functional aneuploidy in

15 multiple cancer types, as defined by the *CIN70* gene signature[9]. It is also part of a 10-gene

16 signature associated with drug resistance, CIN and cell proliferation[10]. Moreover, as part of

17 the 31-gene cell-cycle progression (CCP) signature, it strongly correlates with actively

18 proliferating prostate cancer cells[11]. Likewise, we have shown that *CEP55* is part of a 206

19 gene signature, representing genes enriched in promoting CIN, associated with

20 aggressiveness in triple-negative breast cancer (TNBC)[12].

21   Mechanistically, wild-type *TP53* suppresses CEP55 through PLK1 downregulation

22 and therefore, cancers with *TP53* mutations often have elevated CEP55 levels[13]. In human

23 cancers, CEP55 overexpression results in cell transformation, proliferation, epithelial-to-

24 mesenchymal transition, invasion and cell migration via upregulation of the PI3K/AKT

25 pathway through direct interaction with the p110 catalytic subunit of PI3K[14, 15]. Likewise,

1 CEP55 interacts with JAK2 kinase and promotes its phosphorylation[16]. We have recently

2 shown that *Cep55* overexpression causes male-specific sterility by suppressing Foxo1 nuclear

3 retention through the PI3K/AKT pathway in mice[17]. Furthermore, we showed that CEP55 is a

4 determinant of aneuploid cell fate during perturbed mitosis in breast cancers and could be

5 targeted through MEK1/2-PLK1 inhibition[18]. Moreover, *Cep55* regulates spindle organisation

6 and cell cycle progression in meiotic oocytes[19.] Collectively, these studies highlight the

7 association of CEP55 overexpression with various human malignancies in a context-

8 dependent manner. Though these *in vitro* and clinical correlation studies have so far

9 established the link between CEP55 overexpression and cancer, the underlying mechanism by

10 which CEP55 promotes tumorigenesis *in vivo* remains elusive.

11

12   Here, we report for the first time that *Cep55* overexpression in a mouse model causes

13 high incidence of spontaneous tumorigenesis with a wide spectrum of highly proliferative and

14 metastatic tumours. Notably, *Cep55* overexpression accelerates $Trp53^{+/-}$-induced

15 tumorigenesis. Using mouse embryonic fibroblasts (MEFs), we show that *Cep55*

16 overexpression facilitates rapid proliferation by upregulating multiple cell signalling

17 networks, particularly the PI3K/AKT pathway. Interestingly, we found that *Cep55*

18 overexpression causes both numerical and structural CIN as a consequence of high frequency

19 of anaphase chromatin bridges and micronuclei formation during chromosomal segregation

20 with delayed mitotic exit due to stabilised microtubules. Mechanistically, *Cep55*

21 overexpression compromised the Chk1-dependent S/G2 checkpoint due to hyperactivation of

22 AKT signalling. As a consequence, the *Cep55* overexpressing MEFs cycle faster with

23 increased replication fork speed, replication induced DNA damage and premature mitotic

24 entry. Collectively, our data demonstrate a causal link of overexpressed Cep55 with

25 tumorigenesis, driven through its multiple cellular functions.

1   **Results**

2   ***Cep55 overexpression drives tumorigenesis in vivo***

3   To characterize the pathophysiological role of CEP55 overexpression *in vivo*, we

4   utilised our recently reported transgenic mouse model[17]. Since *Cep55* is highly overexpressed

5   in multiple human cancers irrespective of its role in cell division (Supp. Fig 1), we asked if

6   *Cep55* overexpression causes spontaneous tumorigenesis *in vivo*. We monitored a cohort of

7   wildtype (herein referred to as $Cep55^{wt/wt}$, n=40), heterozygous transgenic ($Cep55^{wt/Tg}$, n=40)

8   and homozygous transgenic ($Cep55^{Tg/Tg}$, n=50) *Cep55* mice over a period of 2.5 years for

9   spontaneous tumour formation. We observed that the $Cep55^{Tg/Tg}$ mice developed various

10   types of tumours at relatively long latencies (median survival 15 months) (Table 1) compared

11   to other well-known oncogenic tumour models (K-ras^{G12D} [20], Pten$^{+/-}$ [21] and Trp53$^{-/-}$ [22, 23]).

12   However, homozygous-*Cep55* overexpressing mice succumbed to cancer significantly earlier

13   (p<0.0001) than $Cep55^{wt/Tg}$ and $Cep55^{wt/wt}$ littermates (Fig 1A). Notably, more than 50% of

14   the $Cep55^{Tg/Tg}$ mice were culled in between 13-15 months due to tumour-associated

15   phenotypes [irreversible weight loss (>15%), change in skin colour, reluctance to move

16   and/or eat] (Supp. Fig 2A), suggesting that these mice might have developed tumours as a

17   result of similar genetic changes caused by *Cep55* overexpression.

18

19   We observed that 70% (35/50) of the $Cep55^{Tg/Tg}$ mice developed a wide spectrum of

20   tumour lesions, including lymphoma, sarcoma, leukaemia and various adenocarcinomas

21   (Fisher exact test p< 0.00001; Fig 1B-D, Supp. Fig 2B and Table 1) compared to only 17.5%

22   (7/40) in $Cep55^{wt/Tg}$ and 5% (2/40) in $Cep55^{wt/wt}$ littermates (Fig 1B). Notably, the tumour

23   burden observed in $Cep55^{Tg/Tg}$ mice varied between 1-3 tumours per animal (Supp. Fig 2C)

24   with tumours originating in multiple tissue types (Supp. Fig 2D) in comparison to $Cep55^{wt/Tg}$,

25   which uniformly developed only adenomas in the lung. Likewise, the $Cep55^{Tg/Tg}$ mice also

1   exhibited a higher incidence of lymphomas, in particular more B-cell lymphoma (1.5-fold)

2   than the T-cell lymphoma (Fig 1D-E, Table 1). IHC staining using B220 (B-cell marker) and

3   CD8 (T-cell marker) specified the incidence of B-cell and T-cell lymphoma's, respectively

4   (Fisher exact test p< 0.0029; Fig 1E-F). Independently, we observed a higher incidence of

5   sarcomas, particularly more haemangiosarcoma than fibrosarcoma (in liver and spleen)

6   (Supp. Fig 2D-E). We also observed a higher incidence of lung and gastric adenocarcinomas

7   compared to other carcinomas (Fig 1G). We also observed a significant increase in

8   hyperplastic lesions (in liver, spleen and endometrium) in $Cep55^{Tg/Tg}$ mice compared to the

9   cohort of other genotypes (Fisher exact test p<0.0001; Supp. Fig 2F).

10

11   The primary cancers observed in the $Cep55^{Tg/Tg}$ mice were highly aggressive in nature

12   with increased proliferation rate, as perceived by the gross morphology and mass of the

13   organs in which these tumours originated (Fig 1C (ii), Supp. Fig 2G). In addition, we

14   observed that ~16% of the mice developed metastases (metastatic carcinoma) in the lungs

15   and liver (Supp. Fig 2H) along with higher levels of inflammatory infiltrates, particularly

16   lymphocytes (data not shown). Collectively, these data highlight that $Cep55$ overexpression

17   alone is sufficient to drive tumorigenesis in mice, causing a broad spectrum of cancers and

18   associated abnormalities, such as inflammation and metastasis.

19

20   ***Cep55 accelerates Trp53$^{+/-}$ induced tumour development in mice***

21   Our data suggests that $Cep55$ overexpression-induced tumorigenesis mimics the

22   tumorigenesis pattern observed in $Trp53^{-/-}$ mice[22], as it induces a significantly higher

23   percentage of lymphomas (~35%) and sarcomas (~17%) (Fig 1D). A previous report has

24   demonstrated that wildtype TP53 restrains CEP55 expression through PLK1[13]. In addition,

25   our clinical data mining suggests that $Cep55$ levels are significantly higher in lung and

1 hepatocellular tumours that exhibit allelic *TP53* copy number loss than in *TP53* diploid

2 tumours (both p<0.0001, Mann-Whitney *U* test) (Supp. Fig 3A). Consistent with this, we

3 observed a high p53 protein level, which is most likely an indication of mutated *Trp53*, in

4 representative $Cep55^{Tg/Tg}$ tumour tissues than normal adjacent tissues (Fig 2A).

5

6   Next, to examine the contribution of *Cep55* overexpression to $Trp53^{+/-}$-induced

7 tumorigenesis, we inter-crossed $Cep55^{Tg/Tg}$ female mice with $Trp53^{-/-}$ male mice to establish

8 bi-transgenic cohorts of $Cep55^{wt/Tg};Trp53^{+/-}$ (n=15), $Cep55^{wt/wt};Trp53^{+/-}$ (n=17),

9 $Cep55^{wt/Tg};Trp53^{+/+}$ (n=11) and $Cep55^{wt/wt};Trp53^{+/+}$ (n=10) mice. These cohorts of mice were

10 monitored regularly for a period of 2.5 years for spontaneous tumour development.

11 Interestingly, we observed that the $Cep55^{wt/Tg};Trp53^{+/-}$ mice succumbed to a broad spectrum

12 of cancer development (spleen, liver and lung) with reduced latency (median survival of 13.8

13 months; p<0.0001) when compared to the $Cep55^{wt/wt};Trp53^{+/-}$ cohort (median survival of 21.6

14 months) (Fig 2B, Supp. Fig 3B-F, Supp. Table 1). Notably, the entire cohort of

15 $Cep55^{wt/Tg};Trp53^{+/-}$ mice exhibited a time frame of tumour development similar to that of

16 $Cep55^{Tg/Tg}$ mice (Fig. 2B), suggesting a strong contribution of Cep55 in inducing $Trp53^{+/-}$

17 mediated tumours.

18

19   Further, the incidence of tumorigenesis observed in $Cep55^{wt/Tg};Trp53^{+/-}$ mice was also

20 significantly higher (~85%; Fisher exact test p<0.0001) in comparison to $Cep55^{wt/wt};Trp53^{wt/-}$

21 (~50%) with 1-3 tumours per animal (Fig 2C). The $Cep55^{wt/Tg};Trp53^{+/-}$ mice also displayed a

22 significantly higher incidence of hyperplastic lesions (Fisher exact test p<0.01) (Fig 2D), and

23 a similar incidence to that observed in $Cep55^{Tg/Tg}$ mice (Supp. Fig 2F). Histopathological

24 analysis indicated the presence of a number of neoplastic lesions (Fig 2E, Supp. Fig 3B,

25 Supp. Table 1) that were similarly observed in $Cep55^{Tg/Tg}$ mice (Fig 1C-D, Supp. Fig 2A and

7

1　　Table 1). Notably, though a similar fractions of $Cep55^{wt/wt};Trp53^{+/-}$ and $Cep55^{wt/Tg};Trp53^{+/-}$

2　　animals developed lymphomas and sarcomas (Fig. 2E), their lymphoma spectrums were

3　　different, in particular there was a higher incidence of B-cell lymphomas than T-cell

4　　lymphomas in the $Cep55^{wt/Tg};Trp53^{+/-}$ mice compared to $Cep55^{wt/wt;}Trp53^{+/-}$ mice (Fig 2F).

5　　Further, the $Cep55^{wt/Tg};Trp53^{+/-}$ mice demonstrate a similar occurrence of fibrosarcoma and

6　　haemangiosarcoma (in liver and spleen), as observed in $Cep55^{Tg/Tg}$ mice (Fig 2G). Taken

7　　together, these data indicate that $Cep55$ overexpression accelerates tumourigenesis and

8　　changes the tumour spectrum in $Trp53^{+/-}$ mice.

9　　***Cep55 overexpression confers a survival advantage through activation of signalling***

10　　***networks***

11　　　　In multiple human cancers, deregulated expression of $CEP55$ has been linked to

12　　enhanced proliferation, migration, invasion, epithelial-mesenchymal transition and

13　　tumorigenesis[4]. To analyse the cellular consequences of $Cep55$ overexpression *in vivo*, we

14　　used primary and spontaneously immortalized MEFs generated from our transgenic mice

15　　(Supp. Fig 4A). We observed significantly higher $Cep55$ transcript and protein levels in the

16　　$Cep55^{Tg/Tg}$ MEFs compared to MEFs from other genotypes (Fig 3A-B). Next, to determine

17　　the growth potential and the senescence rate in the primary MEFs, we performed an NIH-3T3

18　　assay and observed that the $Cep55^{Tg/Tg}$ primary MEFs had a significantly higher proliferation

19　　rate in comparison to $Cep55^{wt/Tg}$ and $Cep55^{wt/wt}$ MEFs, with an increased G2/M proportion of

20　　cells (Fig 3C-D). However, no statistically significant difference was observed in the

21　　proliferation rates between $Cep55^{wt/Tg}$ and $Cep55^{wt/wt}$ (Fig 3C). Likewise, the immortalized

22　　$Cep55^{Tg/Tg}$ MEFs also exhibited similar enhanced proliferative capacity with a significant

23　　difference in cell cycle distributions (Fig 3E-F, Supp. Fig 4B). To define if $Cep55$

24　　overexpression alone could confer enhanced proliferative capacity independent of mitogenic

25　　signals, we serum-starved the primary MEFs of each genotypes and observed higher cell

1   proliferation capacity in *Cep55*$^{Tg/Tg}$ MEFs (~60 hrs) compared to MEFs from other

2   genotypes, highlighting a self-mitogen gaining capability to proliferate and survive in

3   conditions of serum-starvation (Supp. Fig 4C).

4

5   CEP55 has been shown to upregulate AKT phosphorylation through direct interaction

6   with p110 catalytic subunit of PI3 kinase (PI3K) and enhance cell proliferation *in vitro*[14, 15,]

7   [17]. Likewise, we have shown that MYC regulates CEP55 transcriptionally in breast cancer[18].

8   Thus, to characterize the molecular signalling involved in cell proliferation and survival, we

9   investigated the impact of *Cep55* overexpression on Pi3k/Akt - and Erk-dependent signalling

10   networks. Interestingly, immunoblot analysis using whole cell lysates from the MEFs of each

11   genotype demonstrated *Cep55* allele-dependent increase in phosphorylation of Akt^{S473} and its

12   upstream regulator Pdk1^{S241} in *Cep55*$^{Tg/Tg}$ MEFs compared to wild type and heterozygous

13   MEFs (Fig 3G). In addition, we also observed an upregulation of Mapk-dependent signalling

14   molecules, including increased-phosphorylation of Egfr, Erk1/2, Myc and β-catenin, along

15   with increased Pcna, a proliferation marker, in *Cep55*$^{Tg/Tg}$ MEFs (Fig 3G). Similar changes

16   were observed in representative tissue lysates (Supp. Fig 4D). Notably, the effects on the

17   signalling networks were specific to *Cep55* overexpression as knockdown of *Cep55* using

18   two different siRNA oligonucleotides in *Cep55*$^{Tg/Tg}$ MEFs remarkably diminished Pi3k/Akt

19   and Mapk-dependent signalling pathway activities (Fig 3G) and proliferation rate (data not

20   shown). Furthermore, to characterize the role of *Cep55* overexpression in promoting cell

21   proliferation and survival through activated signalling pathways, we used a wide range of

22   Pi3k/Akt, mTor and Erk1/2 pathway-specific inhibitors. Blocking these signalling pathways

23   markedly reduced Cep55 levels suggesting a positive feedback loops between Cep55 and

24   these signalling pathways (Fig 3H). Moreover, we observed that the *Cep55*$^{Tg/Tg}$ MEFs were

25   significantly more sensitive to AKT, PI3K and pan-PI3K-AKT/mTOR inhibitors, but not to

mTOR or Erk1/2 inhibitor treatments alone (Supp. Fig 4E), suggesting a higher dependency of these cells on Pi3k/Akt signalling.

To further decipher the impact of overexpressed *Cep55* on tumorigenesis, we established cell lines from some of the tumours that developed in *Cep55* overexpressing mice (herein abbreviated as tumour cell lines (TCLs)), in particular haemangiosarcoma of the liver (Fig 1C(i)). These cells exhibited a mixed population of bi- and multi-nucleated cells, implying a genomically unstable phenotype (Supp. Fig 4F). Notably, upon transient *Cep55* knockdown using siRNA in the TCL, these cells tended to grow slower with a concomitant reduction in Pdk1 and Akt phosphorylation levels. We only observed a marginal Myc reduction, while there was no impact on Erk1/2 levels (Supp. Fig 4G). Likewise, constitutive *Cep55* knockdown in this line using shRNAs reduced anchorage-independent colony formation (Fig 3I, Supp. Fig 4H), proliferation rate and tumour formation dependent on the extent of reduction of Cep55 levels (Fig 3J, Supp. Fig 4I). Consistently, the *Cep55* knockdown TCL were significantly refractory to PI3K/Akt inhibitor sensitivity (Supp. Fig 4K), suggesting a dependency on PI3K/Akt signalling. Taken together, these data highlight the crucial role of *Cep55* in regulating proliferation and survival-associated signalling networks and its essential function in tumour formation.

Cep55 overexpression promotes structural and numerical chromosomal instability (CIN)

The well-known role of CEP55 as a regulator of CIN is through regulation of cytokinesis[3]. Consistent with this, we found that whole-genome duplicated (WGD) tumours have significantly higher levels of *CEP55* mRNA than diploid and near diploid tumours (Supp. Fig 5A). Likewise, $Cep55^{Tg/Tg}$ MEFs exhibited a three-fold higher percentage (p<0.0001) of binucleated and multinucleated cells (Fig 4A-B). In addition, using FACS

10

1   analysis, we found that both primary and immortalized $Cep55^{Tg/Tg}$ MEFs exhibited a

2   significantly higher percentage of >4n subpopulation (Fig 4C, Supp. Fig 5B). Similar results

3   were observed in different organs isolated from $Cep55^{Tg/Tg}$ mice compared to their littermate

4   counterparts (Supp. Fig 5D). Importantly, we found a significant increase in micronuclei in

5   the $Cep55^{Tg/Tg}$ MEFs (p<0.001) indicating the possible presence of CIN (Fig 4D). Likewise,

6   when $Cep55$ was constitutively knocked down in TCLs, we found a significant reduction in

7   >4n subpopulations (Fig 4E-F, Supp. Fig 5E), suggesting that Cep55 overexpression

8   facilitates CIN. Consistent with this, when we analysed the level of aneuploidy across some

9   of the human cancers using using Genome-wide SNP6 array data from TCGA, we found that

10   $CEP55$ overexpressing tumours show increased structural or numerical aneuploidy, including

11   whole-chromosome aneuploidy and chromosome arm-level aneuploidy (Supp. Fig 6A-D).

12   Additionally, spectral karyotyping of metaphase spreads from $Cep55^{Tg/Tg}$ MEFs demonstrated

13   the presence of significantly higher levels of both numerical and structural chromosomal

14   aberrations compared to other genotypes (Fig 4G). Notably, these MEFs demonstrated

15   complex chromosomal translocations and numerical abnormalities, wherein both $Cep55^{wt/Tg}$

16   and $Cep55^{wt/wt}$ MEFs showed a low level of structural and numerical chromosomal

17   abnormalities (Table 2). In summary, these data highlight that Cep55 overexpression above a

18   certain threshold is sufficient to promote structural and numerical CIN *in vitro* as well as *in*

19   *vivo*.

20

21   ***Cep55 overexpression delays mitotic exit***

22   CIN in cancers primarily occurs due to defective mitosis including unequal

23   chromosome segregation and failure to undergo cytokinesis. Our initial analysis of

24   percentage of cells undergoing mitosis revealed that $Cep55^{Tg/Tg}$ MEFs had a significantly

25   increased mitotic index compared to other genotypes (Supp. Fig 7A-B; p<0.001) and *Cep55-*

1 depleted TCLs showed a reduction in the number of mitotic cells (Supp. Fig 7C). We next

2 asked how *Cep55* overexpression might promote both structural and numerical CIN in these

3 cells during normal and perturbed mitosis. To decipher this, we collected double-thymidine

4 synchronised MEFs for DNA content and time-lapse live-cell imaging analyses. Notably, we

5 observed that the $Cep55^{Tg/Tg}$ MEFs progressed faster through interphase and entered mitosis

6 more rapidly compared to $Cep55^{wt/wt}$ MEFs (Supp. Fig 7D). However, the $Cep55^{Tg/Tg}$ MEFs

7 spent a relatively longer time in mitosis with a higher percentage of cells exhibiting

8 cytokinesis failure compared to wildtype and heterozygous MEFs (Fig 5A-B). Likewise, the

9 $Cep55^{wt/Tg}$ MEFs also spent significantly more time in mitosis compared to wildtype MEFs,

10 indicating an allele-dependent impact of *Cep55* overexpression on mitotic duration (Fig 5A).

11 Multinucleated cells usually take more time to complete mitosis due to high DNA content

12 and the $Cep55^{wt/Tg}$ and $Cep55^{Tg/Tg}$ MEFs exhibited mixed subpopulations of mononucleated,

13 binucleated and multinucleated cells (Fig 4B, C). We therefore performed analysis of

14 individual subpopulations to determine the duration of mitosis (Fig 5C). Surprisingly, along

15 with the bi- and multinucleated $Cep55^{Tg/Tg}$ cells, the mononucleated cells also spent more

16 time in mitosis, indicating that *Cep55* overexpression prolonged mitotic duration

17 independently of DNA content (Fig 5D). Moreover, consistent with our previous report in

18 breast cancer[18], *Cep55* overexpression significantly impacted the duration of time to- and

19 time spent in mitosis upon nocodazole treatment (Fig 5E-F). In particular, the $Cep55^{Tg/Tg}$ cells

20 largely prematurely exited mitosis during nocodazole arrest but the $Cep55^{wt/wt}$ cells

21 predominately died in mitosis (Fig 5G-J). On contrary, the *Cep55*-depleted TCL showed

22 sensitivity towards nocodazole treatment with significant reduction in premature exit and

23 increase in apoptosis (Supp. Fig 7F-H). Therefore, these data indicate that *Cep55*

24 overexpression facilitates CIN through interference with normal cell cycle regulation.

25

1   ***Cep55 overexpression induces defective chromosomal segregation due to stabilised***

2   ***microtubules.***

3   Chromosome segregation errors are a major source for CIN[24]. As we observed that

4   *Cep55*$^{Tg/Tg}$ MEFs demonstrate a higher rate of CIN and homozygous *Cep55*-overexpressing

5   cells spend more time in mitosis compared to cells of other genotypes (Fig 5A-D), we next

6   investigated the impact of *Cep55* overexpression on chromosome segregation during mitosis.

7   Double-thymidine synchronized cells were fixed after ~6hrs post-release and mitotic cells

8   were visualised using fluorescence microscopy. Surprisingly, *Cep55*$^{Tg/Tg}$ MEFs demonstrated

9   a significantly higher frequency ($p<0.05$) of multipolar spindle poles along with unaligned

10   and lagging chromosomes compared to *Cep55*$^{wt/wt}$ MEFs (Fig 6A-D, Supp. Fig 8A-C). In

11   addition, using both fluorescence and live-cell time-lapse microscopy, we also observed that

12   the *Cep55*$^{Tg/Tg}$ MEFs showed significantly higher frequency of anaphase cells with chromatin

13   bridges (anaphase bridges). The presence of anaphase bridges during mitosis indicates the

14   presence of incompletely segregated DNA in *Cep55*$^{Tg/Tg}$ MEFs which in turn result in

15   chromosomal breakage and micronuclei formation (Fig 6E, Supp. Fig 8D). Consistent with

16   this, we observed that the *Cep55*$^{Tg/Tg}$ MEFs exhibited an increased proportion ($p<0.001$) of

17   micronuclei, a morphological characteristic of CIN, when compared to control MEFs (Fig 6F,

18   Supp. Fig 8D).

19

20   Increased kinetochore–microtubule (k-MT) stability causes incomplete segregation of

21   DNA, including lagging chromosomes during anaphase[25, 26]. As CEP55 is recruited to

22   centrosomes and spindle microtubules during mitosis[3] and efficiently bundles microtubules[27],

23   we asked if *Cep55* stabilizes microtubules, and hence increasing segregation errors during

24   mitosis. To analyse spindle microtubule stability, mitotic cells were stained with antibodies

25   that recognize stable detyrosinated- and acetylated-microtubules. *Cep55*$^{Tg/Tg}$ mitotic cells

13

1   exhibited enhanced detyrosinated- and acetylated- microtubule staining compared to mitotic

2   *Cep55$^{wt/wt}$* cells, indicating these cells have stabilised microtubules in spindle poles and

3   midbodies (Fig 6G). Next, to confirm that the generation of chromosome segregation errors,

4   including lagging chromosomes, in response to *Cep55* overexpression is due to stabilised

5   microtubules, we expressed GFP-tagged *KIF2B*, microtubule depolymerizing kinesin-13

6   protein, in both *Cep55$^{Tg/Tg}$* and *Cep55$^{wt/wt}$* MEFs. In particular, exogenous expression of

7   *KIF2B* in *Cep55$^{Tg/Tg}$* cells significantly reduced the frequencies of lagging chromosomes,

8   anaphase bridges and micronuclei (Fig 6H), suggesting that overexpression of *Cep55*

9   stabilises microtubules that in part leads to the mitotic defects observed in these MEFs.

10

11   ***Cep55 overexpression leads to altered Chk1 distribution causing replication stress in an***

12   ***Akt-dependent manner***

13   It has been well established that oncogenes often accelerate DNA replication fork

14   progression and thereby promote GI[28, 29]. We observed that *Cep55*-overexpressing MEFs

15   progressed faster through interphase and entered mitosis more rapidly with enhanced mitotic

16   defects (Fig. 5D and Supp. Fig 7D), including anaphase chromatin-bridge formation that is

17   commonly derived due to replication-associated stress[30]. Since DNA replication is a rate-

18   limiting step during interphase, we therefore investigated the impact of *Cep55* overexpression

19   on replication by examining the replication fork progression rate using DNA fibre assays. We

20   found that the *Cep55*-overexpressing MEFs exhibited a significant increase in replication

21   fork speed (median speed: 1.47kb/min) compared to wildtype cells (median speed:

22   1.03kb/min) (Fig 7A-B). On the contrary, transient silencing of *Cep55* in these cells

23   significantly reduced replication fork speeds, suggesting that *Cep55* overexpression increases

24   proliferation by allowing cells to replicate faster than the *Cep55$^{wt/wt}$* MEFs (Supp. Fig 9A-B).

25   An increase in fork speed by 40% above the normal fork progression speed can induce DNA

1   damage and genome instability[29]. Next, we investigated the impact of increased replication

2   speed on DNA damage in the $Cep55^{Tg/Tg}$ MEFs. Interestingly, we initially observed that the

3   $Cep55^{Tg/Tg}$ MEFs exhibited significantly higher percentage of γ-H2AX positive cells (>5 γ-

4   H2AX foci per cell, Supp. Fig 9C) when compared to the $Cep55^{wt/wt}$ MEFs (Supp. Fig 9D-E).

5   Likewise, we found that $Cep55^{Tg/Tg}$ MEFs have a higher percentage of EdU positive cells

6   (Fig 7C), compared to $Cep55^{wt/wt}$ MEFs. Notably, an increase in the percentage of γ-H2AX

7   positive cells was seen in both Edu-positive and Edu-negative population of the Cep55Tg/Tg

8   MEFs, suggesting that DNA damage is persistent. Despite this increase in baseline damage,

9   no significant differences in DNA damage response signalling were apparent between these

10 lines when cells were challenged with 6-Gy γ-irradiation (Fig 7D). However, we noticed a

11 marked reduction in total Chk1 levels in $Cep55^{Tg/Tg}$ MEFs (Fig 7D). ATR-dependent Chk1 is

12 a well-established effector of DNA damage and replication stress response which is also

13 required for faithful chromosome segregation[31]. Overexpression and/or hyper-activation of

14 AKT has previously been associated with cytoplasmic sequestration of CHK1, hence loss of

15 its checkpoint activity that can ultimately lead to genomic instability[32]. Since $Cep55^{Tg/Tg}$

16 MEFs have highly elevated Akt signalling (Fig 3G), we initially investigated the subcellular

17 Chk1 distribution in MEFs of different $Cep55$ genotypes. Compared to $Cep55^{wt/wt}$ MEFs, the

18 $Cep55^{Tg/Tg}$ MEFs show relatively higher Chk1 levels in cytoplasmic but reduced levels in

19 nuclear fraction (Fig 7E). Meanwhile, treatment of $Cep55^{Tg/Tg}$ MEFs either with PI3K or

20 AKT inhibitor markedly altered the localisation of Chk1 from cytoplasmic to nuclear

21 fraction, confirming that the activation of Akt signalling in $Cep55$-overexpressing cells

22 sequesters Chk1 in the cytoplasmic fraction. To further confirm the involvement of an Akt-

23 mediated checkpoint defect during replication-mediated stress, we treated $Cep55^{Tg/Tg}$ MEFs

24 with either BEZ235 or AKTVII inhibitors and performed DNA fibre assay. Our data showed

25 that treatment of $Cep55$-overexpressing cells with Akt inhibitors significantly reduced

1   replication fork speeds compared to DMSO treated cells (Fig 7F and G and Supp. Fig 9F).

2   AKT phosphorylates CHK1 at serine 280 and impairs its nuclear localization and checkpoint

3   activity independent of ATR[32]. To determine the crucial role of Cep55-Akt-dependent

4   checkpoint deficiency, we transiently reconstituted $Cep55^{Tg/Tg}$ cells with S280A mutant (that

5   cannot be phosphorylated by active-AKT), and $Cep55^{wt/wt}$ cells with S280E mutant (mimics

6   constitutive AKT-dependent phosphorylation). Our data showed that while S280E mutant

7   significantly increased replication fork speed in $Cep55^{wt/wt}$ cells, the S280A mutant

8   reconstituted $Cep55^{Tg/Tg}$ cells on contrary show significantly decreased replication fork speed,

9   suggesting that the checkpoint activity is impaired in Cep55-Akt-dependent manner in these

10   cells (Fig 7H, Supp. Fig). Collectively, our data suggests that overexpression of *Cep55*

11   partially impairs Chk1-mediated checkpoint activation leading to faster replicating cells with

12   persistent DNA damage that undergo an aberrant mitosis, thereby promoting GI in our model.

13

14

16

Discussion

We previously reported a *Cep55*-overexpression mouse model that exhibits male-specific sterility by suppressing Foxo1 nuclear retention through hyperactivation of Pi3k/Akt signalling[17]. In this study, using the same mouse model, we demonstrate for the first time that *Cep55* overexpression causes spontaneous tumorigenesis. Our data highlights the allele-dependent impact of *Cep55* overexpression on cell proliferation and tumorigenesis *in vivo*. The homozygous *Cep55^{Tg/Tg}* mice are prone to develop a wide spectrum of tumours (both solid and haematological origin) with a high incidence rate and high metastasis potential. Interestingly, heterozygous *Cep55^{wt/Tg}* mice developed a lower percentage of adenomas (~20%) and hyperplasia (~8%), suggesting that single copy overexpression of *Cep55* is sufficient to initiate tumorigenesis, although the latency significantly differs between *Cep55^{Tg/Tg}* and *Cep55^{wt/Tg}* mice. Notably, the *Cep55^{Tg/Tg}* mice demonstrated a higher incidence of lymphomas and sarcomas compared to other type of malignancies, mimicking the phenotype observed in *Trp53^{-/-}* mice. As p53 negatively controls CEP55 expression[13], using a bi-transgenic mouse model, we also demonstrated that single copy overexpression of *Cep55* is sufficient to accelerate heterozygous *Trp53^{+/-}* loss-induced tumorigenesis. Interestingly, these data also illustrate that either loss or mutation of *Trp53* might be an early event and a critical secondary hit required for tumour initiation observed in the *Cep55^{Tg/Tg}* mice. Consistent with this, we observed high p53 protein levels, which are most likely an indication of mutated *Trp53*, in representative *Cep55^{Tg/Tg}* tumour tissues than normal adjacent tissues. Notably, partial depletion of *Cep55* (50%) in TCLs significantly delayed tumour initiation and progression, while near-complete depletion (90%) totally impaired tumour initiation in a xenograft model.

As *Cep55* has been linked with GI and its overexpression causes a wide range of tumours *in vivo*, we further characterised GI in *Cep55*-overexpressing cells. *Cep55^{Tg/Tg}* MEFs

17

1   exhibited a high level of cytokinesis failure accompanied by genome doubling. Importantly

2   the $Cep55^{Tg/Tg}$ MEFs showed high level of numerical and structural CIN compared to MEFs

3   of other genotypes. Importantly, in this study, we showed for the first time that $Cep55$

4   overexpression causes mitotic defects including a high frequency of chromatin bridge and

5   micronuclei formation during anaphase. As CEP55 is a microtubule-bundling protein[27],

6   missegregation of chromosomes upon $Cep55$ overexpression might be indicative of

7   kinetochore-microtubule (k-MT) hyperstability. Consistent with this notion, we found that

8   overexpression of $Cep55$ stabilised microtubules and predisposed cells to CIN. Notably,

9   reducing microtubule stability by forced expression of KIF2b in $Cep55^{Tg/Tg}$ MEFs

10 significantly reduced lagging chromosomes. The influence of $Cep55$ overexpression on sister

11 chromatid segregation errors accompanied by cytokinesis failure explains the delayed mitotic

12 exit observed in the $Cep55$-overexpressing cells. Taken together, our data suggests that

13 hyperstabilised microtubules and defective cytokinesis in Cep55-overexpressing cells might

14 be major source of chromosome segregation errors and tetraplodization that can predispose

15 these cells to genomic instability which over time might facilitate tumour development.

16

17   Consistent with previous reports (reviewed by Jeffery et $al.$ [4]), $Cep55$ overexpression

18 led to rapid proliferation. We observed that the $Cep55^{Tg/Tg}$ MEFs displayed hyper-

19 phosphorylated Akt and deregulated downstream PI3K/ Akt signalling such as Gsk-3β, Myc

20 and β-Catenin which might be a further source of genomic instability in these cells. Akt

21 hyperactivation is known to result in cytoplasmic sequestration of Chk1, this might result in a

22 compromised S-phase checkpoint that increases replication fork progression in $Cep55^{Tg/Tg}$

23 MEFs to allow uncontrolled cell cycle progression and consequently promote genomic

24 instability. Consistent with this, overexpression of CHK1 mutant (S280A), that cannot be

25 phosphorylated by overactive AKT, in $Cep55^{Tg/Tg}$ MEFs or their treatment with PI3K/AKT

1   pathway inhibitors resulted in reduced fork-progression. Furthermore, loss of Chk1 function

2   has also been shown to induce chromosomal segregation errors and chromatin-bridges during

3   anaphase resulting in CIN[31, 33], resembling the phenotype we observe.

4   Deregulation of mitotic proteins have long been known to contribute to early cellular

5   transformation and tumorigenesis[34] though they are rarely mutated in cancer [35, 36], but rather

6   prone to amplification. Abnormal expression (loss or gain) of critical mitotic proteins,

7   especially those included in the CIN70 gene signature, such as *MAD2*[37], *BUB1*[38], *AURKA*[39],

8   *EMI1*[40], PLK1[41, 42], *TTK1*[43] and many more, at the genetic level have been shown to induce

9   spontaneous tumorigenesis. The major phenotype observed in these mouse models was

10   defective chromosomal segregation during anaphase which led to CIN and genomically

11   unstable malignancies, similar to the phenotype observed in our model. Thus, the interplay of

12   these mitotic genes with *Cep55* overexpression needs further evaluation. Importantly, in our

13   previous study in breast cancer, we have shown that CEP55 overexpression protects

14   aneuploid cells during perturbed mitosis[17]. We have demonstrated that high level of CEP55

15   significantly induced mitotic slippage in TNBCs as loss of CEP55 enables mitotic cell death

16   by enabling premature mitotic entry upon being challenged with anti-mitotic drugs.

17   Consistently, herein we have demonstrated that Cep55 is a protector of aneuploidy during

18   aberrant mitosis as the aneuploid *Cep55*$^{Tg/Tg}$ MEFs underwent mitotic slippage in response to

19   anti-mitotic drugs and survived mitotic cell death. It also explains the ability of the highly

20   polyploid *Cep55*$^{Tg/Tg}$ MEFs to re-enter mitosis and continue proliferation as Cep55

21   overexpression allows high tolerance and better survival of these cell populations.

22   A recent report has suggested that cells procure specific genomic alterations, mainly

23   impacting the regular function of mitotic genes prior to malignant transformation[44]. CEP55

24   overexpression has been linked with tumorigenesis for a wide-variety of cancers. However,

25   this is the first report to our knowledge demonstrating that overexpression of Cep55 has a

1   causative role in tumorigenesis. Our data clearly demonstrates that Cep55 overexpression

2   beyond a critical level is self-sufficient to induce a wide spectrum of spontaneous tumours.

3   Importantly, we have shown that *Cep55* overexpression leads to induction of pleotropic

4   events such as PI3K/Akt pathway activation, Chk1 sequestration compromising the

5   replication checkpoint, and stabilized microtubules along with chromosomal segregation

6   anomalies which all together causes CIN. Accumulation of these anomalies over time might

7   induce tumourigenesis. In summary, our mouse model could be a valuable tool in studying

8   the mechanism of CIN-associated tumorigenesis and development of CIN-targeting therapies.

9

10

11

1 **Materials and Methods**

2 *Reagents*

3 Nocodozole, BEZ235, BKM120, AZD6244 and AKTVIII were purchased from Selleck

4 Chemicals LCC. Small interfering RNAs (siRNAs) were from Shanghai Gene Pharma.

5 Dulbecco's Modified Eagle's Media (DMEM), Click-iT Alexa Fluor 488 EdU (5-ethynyl-2'-

6 deoxyuridine) imaging kit and Lipofectamine RNAiMAX was purchased from Life

7 Technologies. Foetal Bovine Serum (FBS) was purchased from SAFC Biosciences™,

8 Lenexa, USA. CellTiter 96® AQueous One Solution Cell Proliferation Assay and Dual-Glo®

9 Luciferase Assay were purchased from Promega Corporation.

10

11 *Animal husbandry and ethics statement*

12 All animal work was approved by the QIMR Berghofer Medical Research Institute, Animal

13 Ethics Committee (number A0707-606M) and was performed in strict accordance with the

14 Australian code for the care and use of animals for scientific purposes. The animals were

15 maintained as per the guidelines reported previously[17].

16

17 *Histopathological analysis and immunohistochemistry*

18 For histologic examination, tissues were collected and fixed in 4% formaldehyde in PBS as

19 per the standard protocol described previously[17].

20

21 *Cell Culture and synchronization*

22 To generate the MEFs, mice pregnancy was accessed on the basis of a copulation plug on the

23 following morning post mating date, designated as embryonic day. Such assessment was

24 done for isolating MEFs E13.5 and single cell isolation was performed using the standard

25 protocol described previously[45]. To generate the primary tumor lines (TCLs), tumor was

21

1   surgically removed followed by mechanical disaggregation using a sterile scalpel blade and

2   then incubation in 0.1% collagenase (Sigma Aldrich) in 10 mL of DMEM containing 20%

3   FBS and 1% penicillin-streptomycin (100 U/mL), 1% L-glutamine and cultured in a 25 cm^2

4   tissue flasks. After 24 hrs, the cells were trypsinized and cultured in a new 25 cm^2 tissue flask

5   with media supplemented with 100 µL (100 µg/mL) of EGF, 500 µL (10mg/mL) of insulin

6   and 1% Sodium pyruvate (Life Technology^{TM}. The culture of the murine cell lines was

7   maintained by incubating at 37 ℃ with 20% oxygen levels and 5% CO_2. Cells were

8   synchronized at G1/S by double thymidine block as described previously[46].

9

10   *Genotype analysis and Quantitative real-time PCR*

11   Genotyping, RNA extraction and quantitative real-time PCR was performed using the primer

12   sets used in these assays were used as per the protocol described previously[17].

13   *Immunoblot analysis*

14   The protein extraction from cell lysate or tissue lysate were prepared in urea lysis buffer (8M

15   urea, 1% SDS, 100mM NaCl, 10mM Tris (pH 7.5) and incubated for 30 minutes on ice after

16   which the samples were sonicated for 10 seconds. Western blotting was performed as per the

17   standard protocol and some of the antibodies used for immunoblotting has been described

18   previously[17]. The following are additional antibodies used in this study: γH2AX S139 (05-

19   636); Cell Signaling antibodies: PARP (#9542), pAKT^{S473} (#4060), AKT (#9272), pPdk1^{S241}

20   (#3061), Pdk1(#3062) Chk1 (2G1D5) (#2360), p-GSK-3β$^{(Ser9)}$ (#9336), GSK-3β (#9315), p-

21   Histone H3 (#9706); Millipore antibody: Chk2 (Clone 7) (05-649); BD Pharmingen antibody:

22   β-actin (612656); Bethyl antibody:pKap1$^{(S824)}$ (A300-767A).

23

24   *Cell proliferation assay*

1   The cell proliferation assay using The IncuCyte® S3 Live-Cell Analysis system (Essen

2   BioSciences Inc, USA), as described previously[18]. Doubling time was analyzed at every 12

3   hour interval by counting the overall cell population compared to originally seeded

4   population using the Countess® automated cell counter (Life Technologies[TM]). The NIH-3T3

5   proliferation assay was per performed by using the standard protocol as described

6   previously[45].

7

8   *Colony formation assays*

9   Five hundred to one thousand cells were seeded on 12 well plates and incubated for

10   additional 14 days to determine colony viability. The colonies were fixed with 0.05% crystal

11   violet for 30 minutes as described previously[18].

12

13   *Flow cytometry and cell cycle analysis*

14   Cell cycle perturbations and the subG1 apoptotic fractions were determined using flow

15   cytometry analysis of cells stained with propidium iodide and analyzed using ModFit LT 4.0

16   software as described previously[18].

17

18   *Immunofluorescence*

19   Cells were seeded and incubated overnight on coverslips and were fixed for 15 minutes in 4%

20   paraformaldehyde in PBS, permeabilized in 0.5% Triton X-100-PBS for 15 minutes and

21   blocked in 3% filtered bovine serum albumin (BSA) in PBS. Coverslips with primary

22   antibodies were diluted in blocking solution and incubated overnight at 4°C. Alexafluor

23   conjugated secondary antibodies were diluted 1/300 and DAPI (diluted 1/500 in blocking

24   buffer, stock 1mg/ml), in blocking solution and stained for 45 minutes at 37°C in humidifier

25   chamber. Slides were washed thrice with 0.05% Tween 20 in PBS and mounted in Prolong

1   Gold. Slides were imaged using GE DeltaVision Deconvolution microscope and analyzed

2   using Image J as described previously[18]. Antibodies used for immunofluorescence were:

3   γH2AX S139 (05-636; Millipore), p-Histone H3 (#9706; CST), α-Tubulin (T9026) and γ-

4   Tubulin (T5192).

5

6   *DNA Combing Assay*

7   The DNA fiber protocol was followed as described previously us and others[47, 48]. Cells were

8   labelled with CldU and IdU for 20 minutes each. Progressive replication fork speed was

9   calculated based on the length of the CldU tracks measured using ImageJ software. At least

10   300 replication tracks were analyzed for each sample in two independent experiments. The

11   fork speed was calculated based on conversion factor 1 µm=2.59kb[49].

12

13   *Gene silencing*

14   Transient gene silencing was performed by reverse transfection using 10 nM of respective

15   small interfering   RNAs (siRNAs).   The   sequences   involved   *Cep55*_Scr

16   (5'CAAUGUUGAUUUGGUGUCUGCA3');   *Cep55*_SEQ1   (5'

17   CCAUCACAGAGCAGCCAUUCCCACT 3')   and   *Cep55*_SEQ2   (5'

18   AGCUACUGAGCAGUAAGCAAACAUU). The siRNAs were manufactured by Shanghai

19   Gene Pharma. The transfection was performed using Lipofectamine RNAiMAX (Life

20   Technologies[TM]). Mouse small hairpin RNAs (shRNAs) for Cep55 (pLKO plasmids, (Sigma

21   Aldrich®, St Louis, USA)) clones were established using lentiviral packaging using PEI

22   (Poly -ethyleneimine) solution (Sigma Aldrich®, St Louis, USA).

23   *Cep55*_Scr

24   (5'CCGGCGCTGTTCTAATGACTAGCATCTCGAGATGCTAGTCATTAGAACAGCGT

25   TTTTT3');

1 *Cep55*_sh#1

2 (5'CCGGCCGTGACTCAGTTGCGTTTAGCTCGAGCTAAACGCAACTGAGTCACGGT

3 TTTTG);

4 *Cep55*_sh#2

5 (5'CCGGCAGCGAGAGGCCTACGTTAAACTCGAGTTTAACGTAGGCCTCTCGCTGT

6 TTTTG3');

7 *Cep55*_sh#3

8 (5'CCGGCGTTTAGAACTCGATGAATTTCTCGAGAAATTCATCGAGTTCTAAACGT

9 TTTTT3');

10 *Cep55*_sh#4

11 (5'CCGGGAAGATTGAATCAGAAGGTTACTCGAGTAACCTTCTGATTCAATCTTCT

12 TTTTT3').

13

14 ***Live cell imaging***

15 Live cell imaging for double thymidine releases was performed on an Olympus IX81

16 microscope using excellence rt v2.0 software. Images were analyzed using analySIS LS

17 Research, version 2.2 (Applied Precision) as described previously[50]. Live cell imaging for

18 tracking mitotic defects was performed in H2B Cherry transfected MEFs of each genotype

19 using 20X Andor Revolution WD - Spinning Disk microscope.

20 ***In vivo xenografts***

21 All mice were housed in standard condition with a 12h light/dark cycle and free access to

22 food and water. 2.5×10^6 TLC were prepared in 50% matrigel (BD, Biosciences, Bedford,

23 USA)/PBS and injected subcutaneously injected into the right flank of 6 week old

24 NOD/SCID mice as described previously[18].

25

1   *Bioinformatics analysis*

2   Whole-chromosome (WC) and chromosome arm-level (CAL) somatic copy number

3   aberrations (SCNAs) were inferred from TCGA processed (Level 3) Affymetrix Genome

4   Wide SNP6.0 Array data for the indicated cancer types, as previously described [51]. Using the

5   same datasets, ASCAT2.4 [52] was used to compute the ploidy level for each sample. Samples

6   with ploidy between 1.9 and 2.1 were considered diploid, samples with ploidy lower than 1.9

7   or between 2.1 and 2.5 were called near-diploid aneuploid and samples with ploidy>2.5 were

8   considered aneuploid and having undergone at least one whole-genome doubling (WGD).

9

10   *Statistical analysis*

11   Student's t-test; one-way or two-way ANOVA; RPKM and RSEM with Bonferoni *post hoc*

12   or Mann-Whitney *U* test testing (specified in figure legend) and Fisher exact test was

13   performed using GRAPHPAD PRISM v6.0 (GraphPAd Software, LaJolla, CA, USA) and the

14   p-values were calculated as indicated in figure legends. Asterisks indicate significant

15   difference (*$p<0.05$, **$p<0.01$, ***$p<0.001$ and ****$p<0.0001$), ns= not significant.

16

17

15

21

Conflict of Interest

23   The authors disclose no potential conflicts of interest.

References

1 Zahreddine H, Borden KL. Mechanisms and insights into drug resistance in cancer. *Frontiers in pharmacology* 2013; **4**:28.

2 Perez de Castro I, de Carcer G, Malumbres M. A census of mitotic cancer genes: new insights into tumor cell biology and cancer therapy. *Carcinogenesis* 2007; **28**:899-912.

3 Fabbro M, Zhou BB, Takahashi M *et al.* Cdk1/Erk2- and Plk1-dependent phosphorylation of a centrosome protein, Cep55, is required for its recruitment to midbody and cytokinesis. *Developmental cell* 2005; **9**:477-488.

4 Jeffery J, Sinha D, Srihari S, Kalimutho M, Khanna KK. Beyond cytokinesis: the emerging roles of CEP55 in tumorigenesis. *Oncogene* 2016; **35**:683-690.

5 Frosk P, Arts HH, Philippe J *et al.* A truncating mutation in CEP55 is the likely cause of MARCH, a novel syndrome affecting neuronal mitosis. *Journal of medical genetics* 2017; **54**:490-501.

6 Bondeson ML, Ericson K, Gudmundsson S *et al.* A nonsense mutation in CEP55 defines a new locus for a Meckel-like syndrome, an autosomal recessive lethal fetal ciliopathy. *Clinical genetics* 2017; **92**:510-516.

7 Rawlins LE, Jones H, Wenger O *et al.* An Amish founder variant consolidates disruption of CEP55 as a cause of hydranencephaly and renal dysplasia. *European journal of human genetics : EJHG* 2019.

8 Jeffery J, Neyt C, Moore W *et al.* Cep55 regulates embryonic growth and development by promoting Akt stability in zebrafish. *FASEB J* 2015; **29**:1999-2009.

9 Carter SL, Eklund AC, Kohane IS, Harris LN, Szallasi Z. A signature of chromosomal instability inferred from gene expression profiles predicts clinical outcome in multiple human cancers. *Nature genetics* 2006; **38**:1043-1048.

10 Zhou W, Yang Y, Xia J *et al.* NEK2 induces drug resistance mainly through activation of efflux drug pumps and is associated with poor prognosis in myeloma and other cancers. *Cancer cell* 2013; **23**:48-62.

11 Cuzick J, Swanson GP, Fisher G *et al.* Prognostic value of an RNA expression signature derived from cell cycle proliferation genes in patients with prostate cancer: a retrospective study. *The Lancet Oncology* 2011; **12**:245-255.

12 Al-Ejeh F, Simpson PT, Sanus JM *et al.* Meta-analysis of the global gene expression profile of triple-negative breast cancer identifies genes for the prognostication and treatment of aggressive breast cancer. *Oncogenesis* 2014; **3**:e100.

13 Chang YC, Wu CH, Yen TC, Ouyang P. Centrosomal protein 55 (Cep55) stability is negatively regulated by p53 protein through Polo-like kinase 1 (Plk1). *The Journal of biological chemistry* 2012; **287**:4376-4385.

14 Chen CH, Lu PJ, Chen YC *et al.* FLJ10540-elicited cell transformation is through the activation of PI3-kinase/AKT pathway. *Oncogene* 2007; **26**:4272-4283.

15 Chen CH, Lai JM, Chou TY *et al.* VEGFA upregulates FLJ10540 and modulates migration and invasion of lung cancer via PI3K/AKT pathway. *PloS one* 2009; **4**:e5052.

16 Li M, Gao J, Li D, Yin Y. CEP55 Promotes Cell Motility via JAK2(-)STAT3(-)MMPs Cascade in Hepatocellular Carcinoma. *Cells* 2018; **7**.

17 Sinha D, Kalimutho M, Bowles J *et al.* Cep55 overexpression causes male-specific sterility in mice by suppressing Foxo1 nuclear retention through sustained activation of PI3K/Akt signaling. *FASEB J* 2018; **32**:4984-4999.

18 Kalimutho M, Sinha D, Jeffery J *et al.* CEP55 is a determinant of cell fate during perturbed mitosis in breast cancer. *EMBO Mol Med* 2018; **10**.

19 Xu ZY, Ma XS, Qi ST *et al.* Cep55 regulates spindle organization and cell cycle progression in meiotic oocyte. *Scientific reports* 2015; **5**:16978.

28

20 Jackson EL, Willis N, Mercer K *et al.* Analysis of lung tumor initiation and progression using conditional expression of oncogenic K-ras. *Genes & development* 2001; **15**:3243-3248.

21 Podsypanina K, Ellenson LH, Nemes A *et al.* Mutation of Pten/Mmac1 in mice causes neoplasia in multiple organ systems. *Proceedings of the National Academy of Sciences of the United States of America* 1999; **96**:1563-1568.

22 Donehower LA, Harvey M, Slagle BL *et al.* Mice deficient for p53 are developmentally normal but susceptible to spontaneous tumours. *Nature* 1992; **356**:215-221.

23 Olive KP, Tuveson DA, Ruhe ZC *et al.* Mutant p53 gain of function in two mouse models of Li-Fraumeni syndrome. *Cell* 2004; **119**:847-860.

24 Lee JK, Choi YL, Kwon M, Park PJ. Mechanisms and Consequences of Cancer Genome Instability: Lessons from Genome Sequencing Studies. *Annu Rev Pathol* 2016; **11**:283-312.

25 Bakhoum SF, Kabeche L, Murnane JP, Zaki BI, Compton DA. DNA-damage response during mitosis induces whole-chromosome missegregation. *Cancer Discov* 2014; **4**:1281-1289.

26 Thompson SL, Compton DA. Chromosome missegregation in human cells arises through specific types of kinetochore-microtubule attachment errors. *Proc Natl Acad Sci U S A* 2011; **108**:17974-17978.

27 Zhao WM, Seki A, Fang G. Cep55, a microtubule-bundling protein, associates with centralspindlin to control the midbody integrity and cell abscission during cytokinesis. *Mol Biol Cell* 2006; **17**:3881-3896.

28 Kotsantis P, Petermann E, Boulton SJ. Mechanisms of Oncogene-Induced Replication Stress: Jigsaw Falling into Place. *Cancer discovery* 2018; **8**:537-555.

29 Maya-Mendoza A, Moudry P, Merchut-Maya JM, Lee M, Strauss R, Bartek J. High speed of fork progression induces DNA replication stress and genomic instability. *Nature* 2018; **559**:279-284.

30 Ait Saada A, Teixeira-Silva A, Iraqui I *et al.* Unprotected Replication Forks Are Converted into Mitotic Sister Chromatid Bridges. *Molecular cell* 2017; **66**:398-410 e394.

31 Kabeche L, Nguyen HD, Buisson R, Zou L. A mitosis-specific and R loop-driven ATR pathway promotes faithful chromosome segregation. *Science* 2018; **359**:108-114.

32 Puc J, Keniry M, Li HS *et al.* Lack of PTEN sequesters CHK1 and initiates genetic instability. *Cancer Cell* 2005; **7**:193-204.

33 Petermann E, Woodcock M, Helleday T. Chk1 promotes replication fork progression by controlling replication initiation. *Proc Natl Acad Sci U S A* 2010; **107**:16090-16095.

34 Kops GJ, Weaver BA, Cleveland DW. On the road to cancer: aneuploidy and the mitotic checkpoint. *Nature reviews Cancer* 2005; **5**:773-785.

35 Cahill DP, da Costa LT, Carson-Walter EB, Kinzler KW, Vogelstein B, Lengauer C. Characterization of MAD2B and other mitotic spindle checkpoint genes. *Genomics* 1999; **58**:181-187.

36 Hernando E, Orlow I, Liberal V, Nohales G, Benezra R, Cordon-Cardo C. Molecular analyses of the mitotic checkpoint components hsMAD2, hBUB1 and hBUB3 in human cancer. *International journal of cancer* 2001; **95**:223-227.

37 Sotillo R, Hernando E, Diaz-Rodriguez E *et al.* Mad2 overexpression promotes aneuploidy and tumorigenesis in mice. *Cancer cell* 2007; **11**:9-23.

38 Ricke RM, Jeganathan KB, van Deursen JM. Bub1 overexpression induces aneuploidy and tumor formation through Aurora B kinase hyperactivation. *The Journal of cell biology* 2011; **193**:1049-1064.

39 Fu J, Bian M, Jiang Q, Zhang C. Roles of Aurora kinases in mitosis and tumorigenesis. *Molecular cancer research : MCR* 2007; **5**:1-10.

40 Vaidyanathan S, Cato K, Tang L *et al.* In vivo overexpression of Emi1 promotes chromosome instability and tumorigenesis. *Oncogene* 2016; **35**:5446-5455.

41 Weichert W, Schmidt M, Jacob J *et al.* Overexpression of Polo-like kinase 1 is a common and early event in pancreatic cancer. *Pancreatology : official journal of the International Association of Pancreatology* 2005; **5**:259-265.

42 Ito Y, Miyoshi E, Sasaki N *et al.* Polo-like kinase 1 overexpression is an early event in the progression of papillary carcinoma. *Br J Cancer* 2004; **90**:414-418.

43 Foijer F, Xie SZ, Simon JE *et al.* Chromosome instability induced by Mps1 and p53 mutation generates aggressive lymphomas exhibiting aneuploidy-induced stress. *Proceedings of the National Academy of Sciences of the United States of America* 2014; **111**:13427-13432.

44 Manning AL, Benes C, Dyson NJ. Whole chromosome instability resulting from the synergistic effects of pRB and p53 inactivation. *Oncogene* 2014; **33**:2487-2494.

45 Shi W, Bain AL, Schwer B *et al.* Essential developmental, genomic stability, and tumour suppressor functions of the mouse orthologue of hSSB1/NABP2. *PLoS Genet* 2013; **9**:e1003298.

46 Jeffery JM, Urquhart AJ, Subramaniam VN, Parton RG, Khanna KK. Centrobin regulates the assembly of functional mitotic spindles. *Oncogene* 2010; **29**:2649-2658.

47 Schwab RA, Niedzwiedz W. Visualization of DNA replication in the vertebrate model system DT40 using the DNA fiber technique. *Journal of visualized experiments : JoVE* 2011:e3255.

48 Kalimutho M, Bain AL, Mukherjee B *et al.* Enhanced dependency of KRAS-mutant colorectal cancer cells on RAD51-dependent homologous recombination repair identified from genetic interactions in Saccharomyces cerevisiae. *Mol Oncol* 2017; **11**:470-490.

49 Henry-Mowatt J, Jackson D, Masson JY *et al.* XRCC3 and Rad51 modulate replication fork progression on damaged vertebrate chromosomes. *Molecular cell* 2003; **11**:1109-1117.

50 Jeffery JM, Grigoriev I, Poser I *et al.* Centrobin regulates centrosome function in interphase cells by limiting pericentriolar matrix recruitment. *Cell Cycle* 2013; **12**:899-906.

51 Thangavelu PU, Lin CY, Vaidyanathan S, Nguyen THM, Dray E, Duijf PHG. Overexpression of the E2F target gene CENPI promotes chromosome instability and predicts poor prognosis in estrogen receptor-positive breast cancer. *Oncotarget* 2017; **8**:62167-62182.

52 Van Loo P, Nordgard SH, Lingjaerde OC *et al.* Allele-specific copy number analysis of tumors. *Proceedings of the National Academy of Sciences of the United States of America* 2010; **107**:16910-16915.

53 Rhodes DR, Kalyana-Sundaram S, Mahavisno V *et al.* Oncomine 3.0: genes, pathways, and networks in a collection of 18,000 cancer gene expression profiles. *Neoplasia* 2007; **9**:166-180.

54 Cancer Genome Atlas Research N, Weinstein JN, Collisson EA *et al.* The Cancer Genome Atlas Pan-Cancer analysis project. *Nature genetics* 2013; **45**:1113-1120.

1   **Figure legends**

2   *Figure 1: Cep55 overexpression causes spontaneous tumorigenesis in vivo.*

3   **(A)** Kaplan-Meier survival analysis of mice of indicated genotypes showing that $Cep55^{Tg/Tg}$

4   mice were more susceptible to form tumors compared to their control counterparts; Log-rank

5   (Mantel-Cox) test was performed to determine *P-value* <0.0001.

6   **(B)** Percentage of cancer incidence rate among mice of indicated genotypes (n≥40 per group);

7   Fischer exact test was performed to determine *P-value*<0.0001 (****).

8   **(C)** Representation images of gross morphology (upper panels) and H&E stained microscopic

9   images (lower panels) of selected sections of (i) haemangiosarcoma in liver and (ii) indicated

10 tumor lesions from different organs of tumor-bearing $Cep55^{Tg/Tg}$ mice (scale bars, 200µm).

11 **(D)** Percentage of animals with respective cancer types observed in the transgenic cohorts.

12 **(E)** Percentage of animal with types of lymphomas observed in the respective tumor bearing

13 $Cep55^{Tg/Tg}$ mice. Fischer exact test was performed to determine P-value<0.0029 (***).

14 **(F)** Representative images of B220 and CD8 immunostaining used to categorize the

15 respective types of lymphomas. B220+ve and CD8-ve were classified as B-cell lymphoma

16 while CD8+ve and B220-ve were classified as T-Cell lymphomas (scale bars, 200µm).

17 **(G)** Percentage of adenocarcinoma in the respective organs observed in the tumors bearing

18 $Cep55^{Tg/Tg}$ mice.

19

20 Figure 2: *Heterozygous Cep55 transgenic expression accelerates Trp53$^{+/-}$ induced*

21 *tumorigenesis in mice.* **(A)** Representative images of p53 immunohistochemical staining on

22 tumor sections of respective subtypes observed in the $Cep55^{Tg/Tg}$ mice (bottom panel) in

23 comparison to adjacent normal tissue from the same mice (upper panel).

1   **(B)** Kaplan-Meier survival analysis highlighting the tumor-free survival of the mice of

2   indicated genotypes demonstrating that the *Cep55$^{wt/Tg}$; Trp53$^{wt/-}$* mice were more susceptible

3   to form tumors with a shorter latency period (~14 months) compared to control counterparts;

4   Log-rank (Mantel-Cox) test was performed to determine *P-value* <0.0001.

5   **(C-G)** Percentages of overall cancer incidence **(C),** hyperplastic lesions **(D),** cancer spectrum

6   **(E),** lymphoma **(F)** and sarcoma burden **(G)** among mice of indicated genotypes (n≥10 per

7   group). Fischer exact test was performed to calculate *P-value* <0.0001 (****) and <0.01(**).

8

9   *Figure 3: Cep55 confers survival advantage through signaling networks.*

10   **(A)** Statistical representation of transgenic expression of *Cep55* transcripts observed in the

11   mouse embryonic fibroblasts (MEFs) of respective genotypes (n=3 per group). One-way

12   ANOVA test was performed to determine *P-value* <0.0001 (****) and <0.05(*).

13   **(B)** Immunoblot analysis of Cep55 expression in the whole cell lysates of the primary MEFs

14   of each genotype. β-Actin was used as loading control.

15   **(C)** Statistical representation of NIH-3T3 proliferation assay measured as a function of

16   passage number [indicated as CPD (cumulative population density)] observed in primary

17   *Cep55$^{Tg/Tg}$* MEFs in comparison to its counterparts (n=3 per group). One-way ANOVA test

18   was performed to determine *P-value* <0.0001 (****).

19   **(D)** Statistical representation of the cell cycle profile of primary MEFs of indicated genotype

20   at 24 hours (n=3 per group).

21   **(E)** Statistical representation of the cell viability of immortalized MEFs of each genotype, as

22   indicated in (C), measured per day over a period of 6 days (n=3 per group). One-way

23   ANOVA test was performed to determine *P-value* <0.0001 (****).

24   **(F)** Comparison of cell cycle profile of immortalized MEFs of the indicated genotype over 48

25   hours measured at 12-hour intervals (n=3 per group).

1 **(G)** Immunoblot analysis of the whole cell lysates collected after 24 hours from the

2 immortalized MEF's of indicated genotypes (left panel) and 48 hours from the respective

3 siRNA treated $Cep55^{Tg/Tg}$ MEFs (right panel) indicating the impact of $Cep55$ overexpression

4 on multiple cell signaling pathways. β-Actin was used as loading control.

5 **(H)** Immunoblot analysis of the whole cell lysates collected after 24 hours of treatment with

6 the respecting inhibitors. β-Actin was used as loading control

7 **(I)** Immunoblot analysis of the whole cell lysates collected from the respective isogenic

8 $Cep55$-depleted TCLs at 24 hours validating the levels of Cep55 expression. β-Actin was

9 used as loading control (left panel). Representative images of colony formation at 14 days

10 determined using crystal violet staining in control and $Cep55$-depleted TCLs (right panel).

11 **(J)** Six-week-old female NOD/Scid cohorts of mice were injected subcutaneously with the

12 control and $Cep55$-depleted clones. Growth rates (area, mm^2) of the tumors were measured

13 using a digital caliper. Differences in growth were determined using Student's t-test, P $\leq$

14 0.0001 **(****)**. Graph represents the mean tumor area ± SEM, n = 5 mice/group.

15

16 *Figure 4: Cep55 overexpression promotes chromosomal instability in vivo.*

17 **(A)** Representative images of immunofluorescence demonstrating genomic instability

18 observed in $Cep55^{Tg/Tg}$ MEFs, as indicated by the presence of multiple nuclei (marked by

19 DAPI staining) compared to other counterparts. The cell cytoplasm is marked by α-tubulin

20 (green) (Scale bar, 100μm).

21 (B) Statistical representation showing the percentage of binucleated (left panel) and

22 multinucleated cells (right panel) observed in the respective immortalized MEFs (n=100 cells

23 of each genotype). Error bars represent the ± SD from two independent experiments. One-

24 way ANOVA test was performed to determine *P-value* <0.0001 (****).

1   (C) Statistical representation of polyploidy analysis (>4N DNA contents) determined using

2   FACS analysis in the respective immortalized MEFs. Error bars represent the ± SD from two

3   independent experiments. One-way ANOVA test was performed to determine *P-value* <0.001

4   (***).

5   (D) Representative images showing the presence of micronuclei (marked by DAPI) in the

6   respective immortalized MEFs (left panel) (Scale bar, 100μm). Statistical representation

7   showing the percentage of micronuclei observed in the respective immortalized MEFs (right

8   panel). Error bars represent the ± SD from two independent experiments. One-way ANOVA

9   test was performed to determine *P-value* <0.001 (***).

10   (E) Statistical representation of polyploidy analysis (>4N DNA contents) determined using

11   FACS in the respective sh*Cep55* depleted isogenic clones. Error bars represent the ± SD from

12   two independent experiments. One-way ANOVA test was performed to determine *P-value*

13   <0.001 (***).

14   (F) Statistical representation showing the percentage of binucleated (left panel) and

15   multinucleated cells (right panel) observed in the respective sh*Cep55* depleted isogenic

16   clones. (n=100 cells per clone). Error bars represent the ± SD from two independent

17   experiments. One-way ANOVA test was performed to determine *P-value* <0.0001 (****).

18   (G) Representative metaphases from spectral karyotyping (SKY) in the $Cep55^{Tg/Tg}$ MEFs

19   (passage 25) wherein #1 and #2 denotes biologically independent metaphase representation

20   of $Cep55^{Tg/Tg}$ MEFs.

21

22   *Figure 5: Impact of Cep55 overexpression on mitosis.*

23   (A) Statistical representation showing average time spent in mitosis by the MEFs of indicated

24   genotypes. The MEFs were synchronized using double-thymidine block and released in

25   regular culture media. Individual cells were tracked using bright-field Olympus Xcellence

1 IX81 time-lapse microscopy for overall time taken to complete mitosis from nuclear envelope

2 breakdown up to daughter cell formation, as described previously[18].

3 **(B)** Statistical representation showing the percentage of cytokinesis failure observed in the

4 MEFs of indicated genotypes.

5 **(C)** Statistical representation showing average time spent in mitosis by the different cell

6 population observed among the MEFs of indicated genotypes.

7 **(D)** Statistical representation showing average time spent in mitosis by mononucleated MEFs

8 of indicated genotypes.

9 **(E)** Statistical representation showing comparison of average time spent in mitosis by MEFs

10 of indicated genotypes in presence or absence of nocodazole (0.5 μM). Time in mitosis was

11 calculated as in (A).

12 **(F)** Statistical representation showing comparison of average time taken by the MEFs of

13 indicated genotypes to enter mitosis after release from double-thymidine block, presence and

14 absence of nocodazole (0.5 μM). Time to enter mitosis was calculated as in (A). Error bars

15 represent the ± SD from two independent experiments of all the above expreiments. One-way

16 ANOVA test was performed to determine *P-value* <0.05 (*), <0.01 (**), <0.001 (***) and

17 <0.0001 (****).

18 **(G)** Statistical representation showing the mitotic outcome in the MEFs of indicated

19 genotypes in presence of nocodazole (0.5 μM). Mitotic slippage was defined by premature

20 mitotic exit during nocodazole-induced mitotic arrest, while death was determined through

21 membrane blebbing.

22 **(H)** Statistical representation of the cell cycle profiles of MEFs of indicated genotype in the

23 presence or absence of *nocodazole (0.5 μM)* (n=2 per group).

24 **(I)** Statistical representation of polyploidy analysis (>4N DNA contents) determined using

25 FACS in the indicated immortalized MEFs in the presence or absence of *nocodazole (0.5*

1   *μM)*. Error bars represent the ± SD from two independent experiments. One-way ANOVA

2   test was performed to determine *P-value* <0.0001 (****).

3   **(J)** Statistical representation of percentage SubG1 populations was determined using FACS

4   in the indicated immortalized MEFs in the presence or absence of *nocodazole (0.5 μM)* (n=3

5   per group). Error bars represent the ± SD from two independent experiments. One-way

6   ANOVA test was performed to determine *P-value* <0.0001 (****).

7

8   *Figure 6: Cep55 overexpression causes various mitotic defects.*

9   **(A-F)** Representative images of immunofluorescence **(A)** and quantification and statistical

10   analyses. n=50 cells per experiment were counted and the experiment was repeated twice

11   across each genotype (Scale bar, 100μm). **(B-F)** of mitotic defects observed in wildtype and

12   transgenic MEFs as indicated by the presence of tripolar spindle poles, unaligned metaphase

13   plates, lagging chromosomes, as well as chromatin bridges and micronuclei. Error bars

14   represent the ± SD from two independent experiments. Student's t-test was performed to

15   determine *P-value* <0.05 (*) and <0.01 (**).

16   **(G)** Representative images of detryosinated (red) and acetylated tubulin of both anaphase and

17   midbody cytokinetic bridges showing stabilized tubulin in *Cep55$^{Tg/Tg}$* MEFs. n=50 cells per

18   experiment were counted and the experiment was repeated twice across each genotype (Scale

19   bar, 100μm).

20   **(H)** Statistical representation showing reduction in mitotic defects (described previously in

21   A-F) upon *KIF2B* overexpression in the MEFs of indicated genotypes. Error bars represent

22   the ± SD from two independent experiments. Student's t-test was performed to determine *P-*

23   *value* <0.05 (*) and <0.01 (**).

24

25

1 *Figure 7: Cep55 overexpression causes replication stress.*

2 **(A, B)** Statistical representation of velocity of progressing forks **(A)** and distributions of

3 replication fork speeds **(B)** was determined using DNA fiber analysis. Indicated MEFs were

4 pulsed labeled with IdU (red) and CldU (green) for 25 minutes and the fibers were imaged

5 and quantified. Representative images of respective genotypes are shown on the right hand

6 panel. At least 300 fibers from each cell line were analysed from two independent

7 experiments with error bars representing the standard error of the mean (SEM). Unpaired t

8 test with and without Welch's correction between two groups was used to determine the

9 statistical *P-value*, <0.0001 (****).

10 **(C)** Representative images of immunofluorescence of EdU (S-phase cells) positivity (green)

11 allowed to label for an hour alongside double stranded marker yH2ax (red) observed in the

12 MEFs of indicated genotypes are shown on the left hand panel. DNA was marked using

13 DAPI (blue). The statistical representation of the percentages of EdU positive cells; γh2ax in

14 EdU positive or negative cells are demonstrated in the right hand side panel. Error bars

15 represent the ± SD from two independent experiments. Student's t-test was performed to

16 determine *P-value* <0.001 (***) and <0.0001 (****).

17 **(D)** Immunoblot analysis of the whole cell lysate from respective MEFs highlighting the

18 presence of indicated proteins in cells of indicated genotypes after challenged with 6-Gy

19 irradiation. β-Actin was used as loading control.

20 **(E)** Immunoblot analysis of cytoplasmic-nuclear fractionation was performed to determined

21 Chk1 protein distributions with and without indicated inhibitor treatments. Cells were treated

22 for 6 prior to the assay. H3 and Vinculin were used as loading control in each fraction.

23 **(F, G)** Statistical representation of velocity of progressing forks **(F)** and distributions of

24 replication fork speeds **(G)** was determined using DNA fiber analysis as described in A.

25 *Cep55*$^{Tg/Tg}$ MEFs were pretreated for 6 hours with indicated inhibitors and forks speeds were

1   determined. Representative images are shown on the right. At least 300 fibers from each cell

2   line were analysed from two independent experiments with error bars representing the

3   standard error of the mean (SEM). One way ANOVA with Brown-Forsythe test was used to

4   determine *P-value* <0.0001 (****).

5   **(H)** Left: Immunoblot analysis showing transiently transfected mutants Chk1 along with

6   Cep55. β-Actin was used as loading control. Right: Statistical representation of velocity of

7   progressing forks as indicted in A. Both cell lines were transiently transfected with 1.5µg

8   indicated mutant constructs respectively (CHK1-S280A and S280E) for 24 h and DNA fiber

9   analysis and immunoblotting were performed. For fiber assays, at least 150 fibers from each

10   cell line were analysed from two independent experiments with error bars representing the

11   standard error of the mean (SEM). One way ANOVA with Brown-Forsythe test was used to

12   determine *P-value* <0.0001 (****).

13

14

15

16

17

18

19

20

21

22

23

24

25

1 **Supplementary figure legends**

2

3 ***Supp. Fig1: CEP55 is overexpressed in a broad range of cancers independent of a***

4 ***proliferation-associated effect.***

5 **(A)** CEP55 expression in multiple data sets of various cancer types, analyzed using the

6 Oncomine database[53]. Overall, 7403 tumor samples to 1467 normal control samples of

7 matched tissue type were compared and we observed that the expression of *CEP55* to be

8 significantly higher than in matched normal tissue. A total of 212 data sets were identified

9 showing statistically significant deregulated expression of CEP55 in tumours compared to

10 matched normal control tissues. Each box represents a dataset. Studies showing significant

11 CEP55 overexpression are shown in red, those showing significant underexpression in blue.

12 Fold over- or under-expression is shown as indicated.

13 **(B)** Pie charts derived from the dataset described in (A) implying significant CEP55

14 expression differences compared to normal tissue (n=212) wherein 193 case studies (91%)

15 illustrated significant overexpression, while 19 case studies (9%) showed significant

16 underexpression. Proportion of studies showing significant overexpression (red) and

17 underexpression (blue) is shown. Fisher's exact tests was used to determine the respective *P*-

18 values.

19 **(C)** RSEM-normalised CEP55 expression levels, performed using the TCGA[54] dataset, in

20 lung adenocarcinoma (LUAD), liver hepatocellular carcinoma (LIHC) and or colorectal

21 adenocarcinoma (COADREAD) samples compared to matched normal control samples.

22 Collectively, the datasets illustrate that *CEP55* is significantly upregulated in respective

23 tumors in comparison to normal control tissue. Student t' tests was used to determine *P-value*

24 <0.0001 (****).

1   (**D**) Ratios of CEP55/MKI67 (upper panel) and CEP55/PCNA (lower panel) RSEM-

2   normalised expression levels in LUAD, LIHC and COADREAD of datasets as in (C).

3   (**E**) Representation of the tumors that express MKI67 at levels in the same range as normal

4   samples show significantly elevated CEP55 expression levels than the normal samples. These

5   data illustrate that expression of CEP55 is significantly higher in tumors than in normal

6   tissue, even after compensation for the expression of the cell proliferation markers Ki67

7   (upper panel) or PCNA (lower panel), indicating that CEP55 expression in tumors is cell

8   cycle-independent. Mann-Whitney *t*- test was used to determine *P-value* <0.0001(****).

9

10   *Supp. Fig2:* **Spontaneous tumourigenesis induced by *Cep55* overexpression *in vivo*.**

11   (**A**) Statistical representation of the body weight observed at the end of tumor survival of

12   each genotype (n>40 per group). Error bars represent the ± SEM from the entire experimental

13   cohort. One-way ANOVA test was performed to determine *P-value* <0.0001 (****).

14   (**B**) Representation of H&E-stained microscopic images indicated tumor lesions from

15   different organs of tumors-bearing $Cep55^{Tg/Tg}$ mice; (scale bars, 200µm).

16   (**C-F**) Statistical representation of the overall distribution of indicated tumour lesions among

17   respective major organs of tumour-bearing $Cep55^{Tg/Tg}$ mice (HCC=hepatocellular carcinoma).

18   Percentage of tumor burden (**C**), types of tumors that they originated from (**D**), Sarcoma (**E**)

19   and hyperplasia (**F**) observed in tumour-bearing $Cep55^{Tg/Tg}$ mice.

20   (**G**) Statistical representation of the respective weights of spleen, liver and lung observed in

21   the indicated genotypes at the end of their respective survival. Error bars represent the ± SEM

22   from the entire experimental cohort. One-way ANOVA test was performed to determine *P-*

23   *value* <0.0001 (****).

24   (**H**) Percentage of metastasis incidence observed in the tumor bearing $Cep55^{Tg/Tg}$ mice.

25

1 *Supp. Fig3:* **Loss of Trp53 leads to early tumor latency in *Cep55* overexpressing mice.**

2 **(A)** Boxplots showing CEP55 expression in indicated tumors or matched normal samples

3 with *TP53* copy number and/or mutation status as indicated. Numbers of samples for each

4 column are shown above the x-axis. *P*-values were determined using Mann-Whitney *t*- test.

5 ****p<0.0001.

6 **(B)** Representation of H&E stained microscopic images of selected sections of indicated

7 tumors lesions from different organs of tumor-bearing mice of respective genotypes; (scale

8 bars, 200μm).

9 **(C)** Percentage of the overall distribution of indicated tumor lesions among respective major

10 organs of tumor-bearing mice of indicated genotypes.

11 **(D)** Percentage of number of tumors (tumour burden) observed in each mice of respective

12 genotypes.

13 **(E)** Statistical representation of the body weight observed at the end of tumor survival of each

14 genotype (n≥10 per group). Error bars represent the ± SEM from the entire experimental

15 cohort. One-way ANOVA test was performed to determine *P-value* <0.0001 (****).

16 **(F)** Statistical representation of the respective weights of spleen, liver and lung observed in

17 the indicated genotypes at the end of their respective survival. Error bars represent the ± SEM

18 from the entire experimental cohort. One-way ANOVA test was performed to determine *P-*

19 *value* <0.0001 (****).

20

21 *Supp. Fig4:* **Cep55 overexpression promotes cell proliferation advantage *in vivo*.**

22 **(A)** Representation of genotyping of DNA isolated from the primary MEFs of each indicated

23 genotype using PCR, showing the presence of amplicons of the expected size for each

24 genotype. #1 and #2 denotes biologically independent DNA samples of each genotype.

1 **(B)** Statistical representation of relative fold change in the doubling time of immortalized

2 MEFs from each genotype as indicated in (C) (n=3 per group). Error bars represent the $\pm$

3 SEM from the entire experimental cohort. One-way ANOVA test was performed to

4 determine *P-value* <0.001.

5 **(C)** Statistical representation of cell proliferation observed in the immortalized MEFs of

6 indicated genotype at different time points during serum starved conditions (n=3 per

7 experiment). One-way ANOVA test was performed to determine *P-value* <0.0001.

8 **(D)** Immunoblot analysis of indicated whole tissue lysates of respective genotypes of six-

9 month old littermates. β-Actin was used as loading control.

10 **(E)** Statistical representation of the cell viability of the immortalized MEFs of each genotype

11 after 48hrs of treatment with indicated small molecule inhibitors treated as per the designated

12 concentration. (n=2 per group). Error bars represent the $\pm$ SEM from the entire experimental

13 cohort. One-way ANOVA test was performed to determine *P-value* not significant (ns),

14 <0.05 (*) and <0.01 (**).

15 **(F)** Representative images of cell morphology (bright field image; fluorescence image

16 wherein α-tubulin (green) marks the cytoplasm while DAPI (blue) marks the nucleus) of the

17 TCLs isolated from the haemangiosarcoma found in (Fig1 Ci). The red arrow indicated

18 presence of multinucleated cells while the white arrow represents presence binucleated cells.

19 **(G)** Immunoblot analysis of the whole cell lysate of TCLs to assess the levels of indicated

20 signaling molecules following transient depletion of *Cep55* using *siCep55* (10 nM, S1). β-

21 Actin was used as loading control (left panel). Effect of Cep55 depletion using siCep55 (10

22 nM) on cell proliferation, assessed using the IncuCyte ZOOM® live-cell imager. The

23 percentage of cell confluence was determined using an IncuCyte mask analyser (right panel).

24 Error bars represent the $\pm$ SD from two independent experiments. Student t' test was

25 performed to determine *P-value* <0.01 (**).

(H) Immunoblot analysis of whole-cell lysates of TCLs to validate extent of *Cep55* depletion with indicated sh*Cep55* sequences (indicated as #S1- #S4 with sh_Scr as control) in the TCLs. β-Actin was used as loading control.

(I) Effect of *Cep55* depletion on cell proliferation in TCLs assessed as described in (G). Error bars represent the ± SD from two independent experiments. Student t' test was performed to determine *P-value* <0.01 (**).

(J) Statistical representation of the cell cycle profile of respective TCL clones (n=2 per group).

(K) Statistical representation of the cell viability of the indicated TCL clones after 48hrs of treatment with indicated small molecule inhibitors treated as per the designated concentration. (n=2 per group). Error bars represent the ± SEM from the entire experimental cohort. One-way ANOVA test was performed to determine *P-value* not significant (ns), <0.05 (*) and <0.01 (**).

Supp. Fig5: **Cep55 overexpression causes genomic instability.**

(A) Boxplots showing CEP55 expression in tumors whose genomes are diploid, near-diploid aneuploid or aneuploid after whole-genome doubling (WGD). Data are from the TCGA liver hepatocellular carcinoma (LIHC), lung squamous cell carcinoma (LUSC), lung adenocarcinoma (LUAD) and colorectal adenocarcinoma (COADREAD) datasets. Mann-Whitney *U* tests was used to determine *P-value* <0.05 (*), <0.01 (**), <0.001 (***), <0.0001 (****).

(B) Statistical representation of polyploidy analysis (>4N DNA content) determined using FACS in the respective primary MEFs of each genotype. Error bars represent the ± SD from the entire experimental cohort. One-way ANOVA test was performed to determine *P-value* <0.001 (***).

1 **(C)** Statistical representation showing comparison of overall polyploidy analysis (>4N DNA

2 content) between primary and immortalized *Cep55*$^{Tg/Tg}$ MEFs. Error bars represent the ± SD

3 from the entire experimental cohort. One-way ANOVA test was performed to determine *P-*

4 *value* <0.001 (***).

5 (**D**) Statistical representation of overall polyploidy analysis observed in the indicated tissues

6 of respective age-matched mice of each genotype. Error bars represent the ± SD from the

7 entire experimental cohort. One-way ANOVA test was performed to determine *P-value*

8 <0.0001 (****).

9 **(E)** Immunofluorescence showing genomic instability observed among the respective

10 sh*Cep55*-depleted isogenic clones as indicated by the presence of multiple nuclei (marked by

11 DAPI staining) compared to counterparts. The entire cell (cytoplasm) was marked by α-

12 tubulin (green), while the centrosomes were marked by γ-tubulin (red) (Scale bar, 100μm).

13

14 *Supp. Fig6:* **Association of CEP55 overexpression with aneuploidy.**

15 **(A)** Boxplots representation showing CEP55 expression in indicated tumors with whole-

16 chromosome (WC)-euploid and WC-aneuploid genomes. The data was defined using the

17 TCGA LIHC, LUSC, and LUAD datasets (described in Supp. Fig5A)[51].

18 **(B)** Boxplots as in (A) but at the chromosome arm level (CAL).

19 **(C)** Boxplots representation demonstrating the chromosome arm-level (CAL) aneuploidy,

20 i.e., total number of chromosome arms gained or lost per sample, with respect to the highest

21 (hi) and lowest (lo) CEP55 mRNA expression quartiles from TCGA RNAseq data.

22 **(D)** Boxplots representation demonstrating the whole-chromosome (WC) aneuploidy, i.e., the

23 total number of whole chromosomes gained or lost per sample, with respect to the highest

24 (hi) and lowest (lo) CEP55 mRNA expression quartiles from TCGA RNAseq data. For all of

25 the above, Mann-Whitney U tests was used to determine *P-value*.

1   *Supp. Fig7:* **Mitotic cell fate in Cep55 overexpressing MEFs.**

2   **(A)** Representative images of immunofluorescence demonstrating mitotically active cells

3   observed in *Cep55$^{Tg/Tg}$* MEFs as compared to other counterparts. Mitotic cells are marked by

4   phospho-histone H3 (green) and the nucleus is marked by DAPI (blue). Scale bar, 100μm

5   (left panel). Statistical representation of phospho-histone H3^{+ve} cells in the MEFs of indicated

6   genotypes (right panel). Error bars represent the ± SD from the entire experimental cohort.

7   One-way ANOVA test was performed to determine *P-value* not significant (ns), <0.001

8   (***).

9   **(B)** Statistical representation of mitotic index (number of rounded cells/overall cells in an

10 area) observed in the MEFs of indicated genotypes using bright field Olympus Xcellence

11 IX81 time-lapse microscopy per-field. Overall, 300 cells were counted (~40 cells per field) of

12 each genotype. Error bars represent the ± SD from the entire experimental cohort. One-way

13 ANOVA test was performed to determine *P-value* not significant (ns), <0.01 (**).

14 **(C)** Statistical representation of phospho-histone H3^{+ve} cells observed in the respective

15 sh*Cep55* depleted isogenic clones. Error bars represent the ± SD from the entire experimental

16 cohort. One-way ANOVA test was performed to determine *P-value* not significant (ns),

17 <0.001 (***).

18 **(D)** Data showing the cell cycles profiles of MEFs of indicated genotype. The cells were first

19 synchronized by double-thymidine block and released in regular culture media following

20 which, they were collected after 2-hour intervals. Error bars represent the ± SD from the

21 entire experimental cohort.

22 **(E)** Statistical representation showing the percentage of binucleated (left panel) and

23 multinucleated cells (right panel) observed in the respective MEFs of indicated genotypes

24 calculated using time-lapse microscopy (n=100 cells of each genotype). Error bars represent

45

1   the ± SD from the entire experimental cohort. One-way ANOVA test was performed to

2   determine *P-value* <0.05 (*), <0.01 (**), <0.001 (***).

3   **(F)** Statistical representation of the cell cycle profile of the respective sh*Cep55* depleted

4   isogenic clones in the presence or absence of *nocodazole (0.5 μM)* (n=2 per group).

5   **(G)** Statistical representation of polyploidy analysis (>4N DNA contents) determined using

6   FACS in the respective sh*Cep55* depleted isogenic clones in presence or absence of

7   *nocodazole (0.5 μM).* Error bars represent the ± SD from the entire experimental cohort.

8   One-way ANOVA test was performed to determine *P-value* <0.0001 (****).

9   **(H)** Statistical representation of percentage SubG1 population was determined using FACS in

10   the respective sh*Cep55* depleted isogenic clones in presence or absence of *nocodazole (0.5*

11   *μM)* Error bars represent the ± SD from the entire experimental cohort. One-way ANOVA

12   test was performed to determine *P-value* <0.0001 (****).

13

14   ***Supp. Fig8: Cep55 overexpression causes mitotic defects.***

15   **(A, B)** Representative images showing normal **(A)** and perturbed mitoses **(B)**. Individual cells

16   were tracked using bright-field Olympus Xcellence IX81 time-lapse microscopy and mitotic

17   anomalies were determined (Scale bar, 100μm).

18   ***Supp. Fig9: Cep55 overexpression causes replication stress.***

19   Statistical representation of velocity of progressing forks **(A)** and distributions of replication

20   fork speeds **(B)** was determined using DNA fiber analysis upon *Cep55* knockdown in

21   *Cep55$^{Tg/Tg}$* MEFs. At least 300 fibers from each cell line were analysed from two independent

22   experiments with error bars representing the standard error of the mean (SEM). Unpaired t

23   test with and without Welch's correction between two groups was used to determine the

24   statistical *P-value*, <0.0001 (****).

1   **(C)** Representative images of immunofluorescence (left panel) demonstrating presence of

2   DNA damage marked by γH2ax (green) observed in indicated genotypes (Scale bar, 100μm).

3   Statistical representation showing percentage of γH2ax positive cells (>5 foci of yH2ax/cell)

4   in the MEFs of indicated genotypes MEFs (right panel)**.** Error bars represent the ± SD from

5   the entire experimental cohort. One-way ANOVA test was performed to determine *P-value*

6   <0.01 (**).

7   **(E)** Immunoblot analysis of indicated proteins in cells challenged with 6-Gy irradiation. β-

8   actin was used as loading control.

A.

Survival (%) vs Time (in years)

Cep55$^{wt/wt}$
Cep55$^{wt/Tg}$
Cep55$^{Tg/Tg}$

p<0.0001

B.

Tumour incidence rate (%)

Cep55: wt, wt/Tg, Tg/Tg

****

D.

Figure 1

Animals with tumours (%)

Lymphoma, Sarcoma, Leukemia, Adenoma, Carcinoma

C.

(i) Haemangiosarcoma (ii) T-Cell Lymphoma   Hepatocellular carcinoma   Lung Adenocarcinoma

wt/wt

Tg/Tg

H&E

200μm   200μm   200μm   200μm

E.

Lymphoma (%)

B-Cell, T-Cell

***

F.

B-Cell Lymphoma   T-Cell Lymphoma

B220 +ve   CD8 +ve

200μm   200μm

CD8 -ve   B220-ve

200μm   200μm

G.

Adenocarcinoma (%)

Lung, Hepactic, Papillary, Gastric

Figure 2

A.

T-Cell Lymphoma   B-Cell Lymphoma   Haemangiosarcoma   T-Cell Lymphoma

Adjacent tissue

Tumour

B.

Survival (%)

Time (Years)

p<0.0001

$Cep55^{wt/wt}/Tp53^{+/+}$
$Cep55^{wt/Tg}/Tp53^{+/+}$
$Cep55^{wt/wt}/Tp53^{+/-}$
$Cep55^{wt/Tg}/Tp53^{+/-}$

C.

Animals with tumors %

****

Cep55   wt   wt/Tg   wt   wt/Tg
Tp53   +/+   +/+   +/-   +/-

D.

Hyperplasia (%)

**

Cep55   wt   wt/Tg   wt   wt/Tg
Tp53   +/+   +/+   +/-   +/-

E.

Animals with tumors (%)

Lymphoma   Sarcoma   Leukemia   Adenor-   Carcinoma

F.

Animals with tumors (%)

T-Cell Lymphoma
B-Cell Lymphoma

Cep55   wt   wt/Tg
Tp53   +/-   +/-

G.

Animals with tumors (%)

Fibrosarcoma
Haemagiosarcoma
Leiomyosarcoma

Cep55   wt   wt/Tg
Tp53   +/-   +/-

Figure 3

Figure 4

Figure 5

Figure 6

Figure 7

A.

Fork Speed(Kb/min)

****

$Cep55$ wt Tg/Tg

B.

- $Cep55^{wt/wt}$
- $Cep55^{Tg/Tg}$

% forks (frequency)

Fork speed (kb/min)

wt/wt

Tg/Tg

C.

EdU γh2ax DAPI Merged

$Cep55^{wt/wt}$

$Cep55^{Tg/Tg}$

% Edu^{+ve} Cells   ***

$Cep55$ wt Tg/Tg

% Edu^{+ve} γH2ax^{+ve} Cells   ****

$Cep55$ wt Tg/Tg

% Non-Edu^{+ve} γH2ax^{+ve} Cells   ****

$Cep55$ wt Tg/Tg

D.

	$Cep55^{wt/wt}$					$Cep55^{Tg/Tg}$				
Hr	0	1	3	6	12	0	1	3	6	12

Cep55
Nbs1
pKap1
Chk1
Chk2
γH2AX
β-Actin

E.

	$Cep55^{wt/wt}$		$Cep55^{Tg/Tg}$		DMSO		PI3Ki		AKTi	
	Cyto	Nuc	Cyto	Nuc	Cyto	Nuc	Cyto	Nuc	Cyto	Nuc

Cep55
p-Akt$^{(S473)}$
Akt
Chk1
Vinculin
H3

F.

Fork Speed(Kb/min)

****

DMSO   BEZ235   AKTViii

G.

% forks (frequency)

Fork speed (kb/min)

H.

wt/wt Tg/Tg

mock S280E mock S280A

Cep55
Chk1
β-Actin

Fork Speed(Kb/min)

****   ****

mock S280E mock S280A

$Cep55$ wt/wt Tg/Tg

Table 1: Distribution of cancer spectrum in *Cep55* transgenic mice.

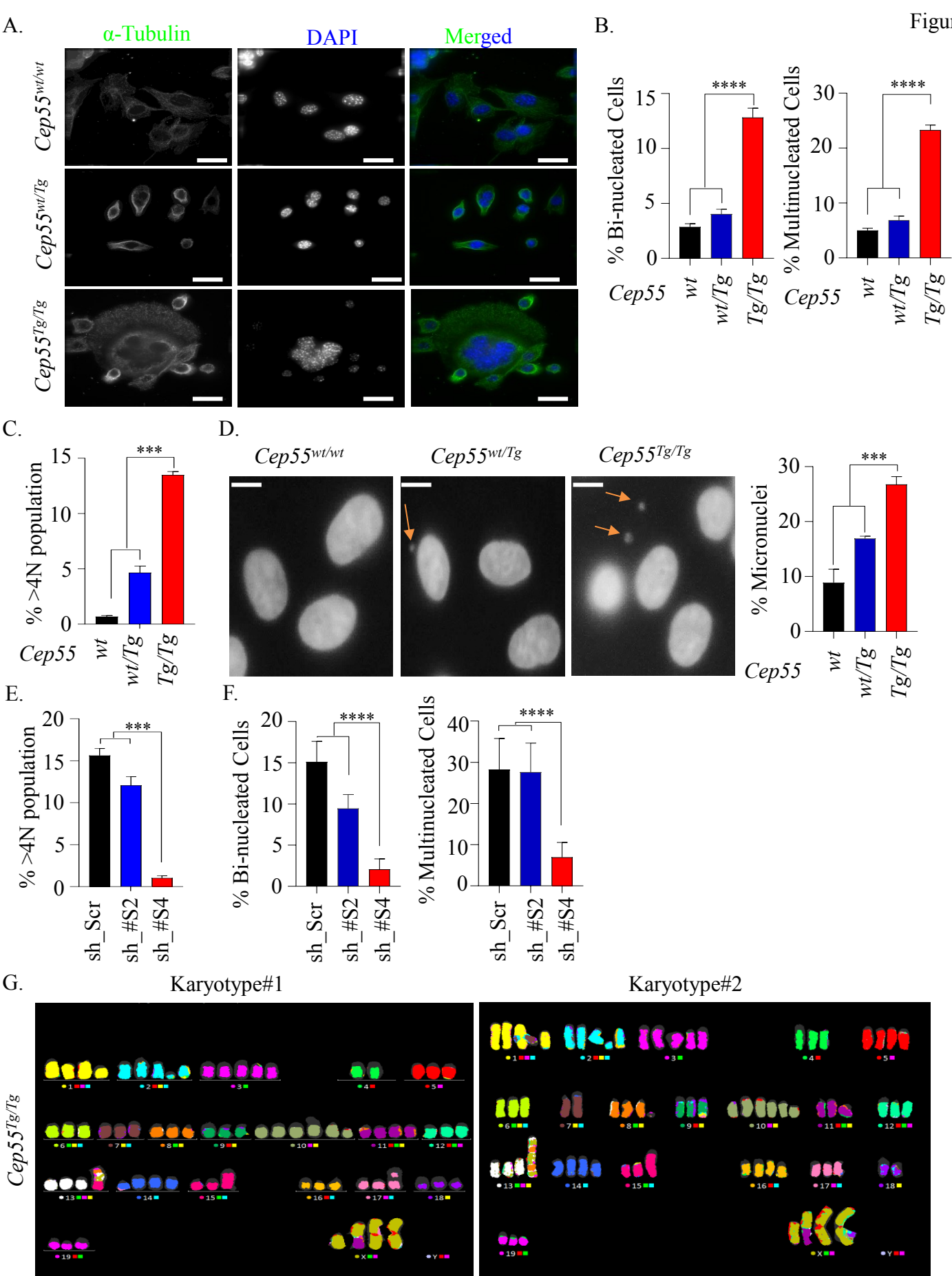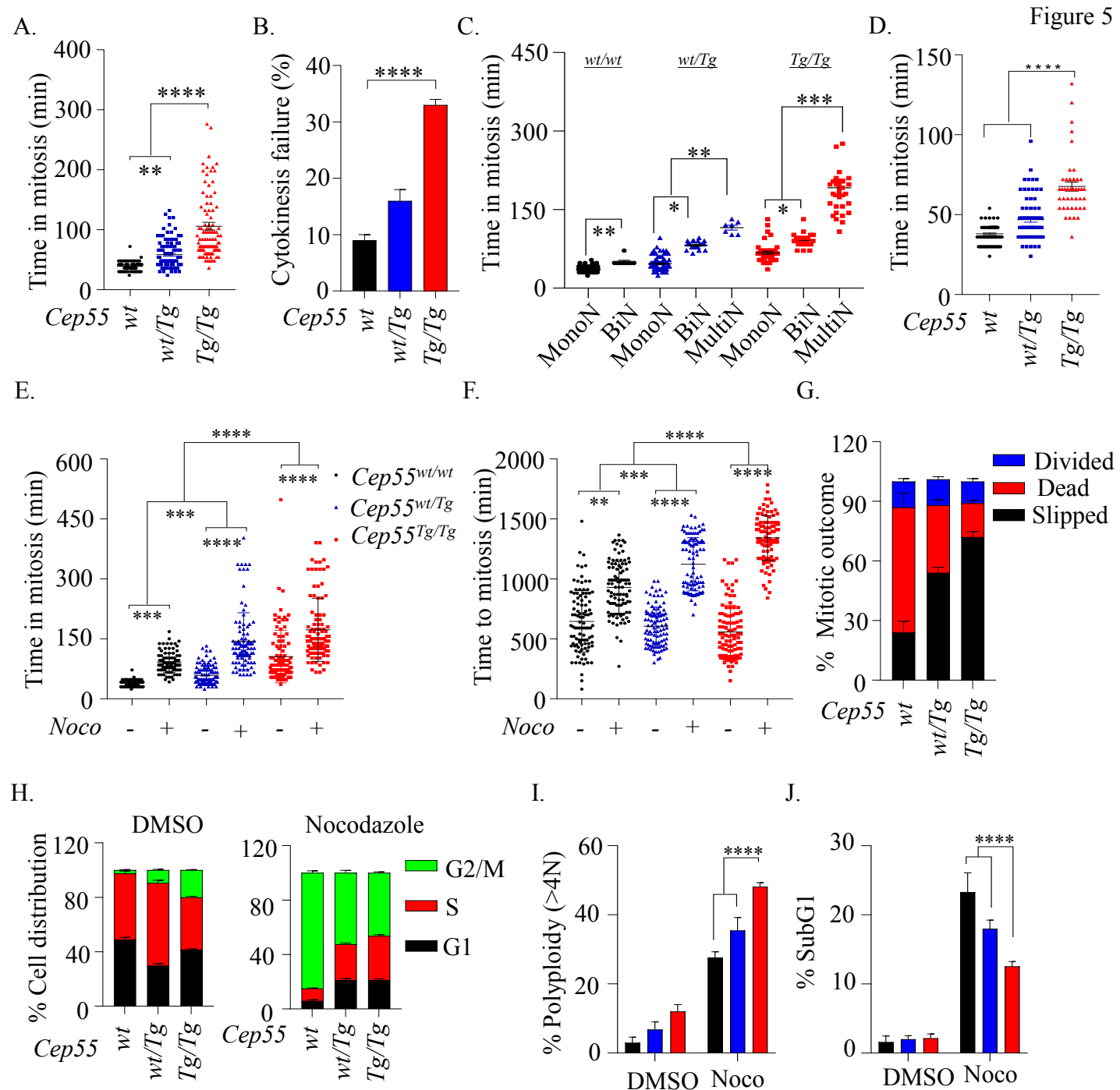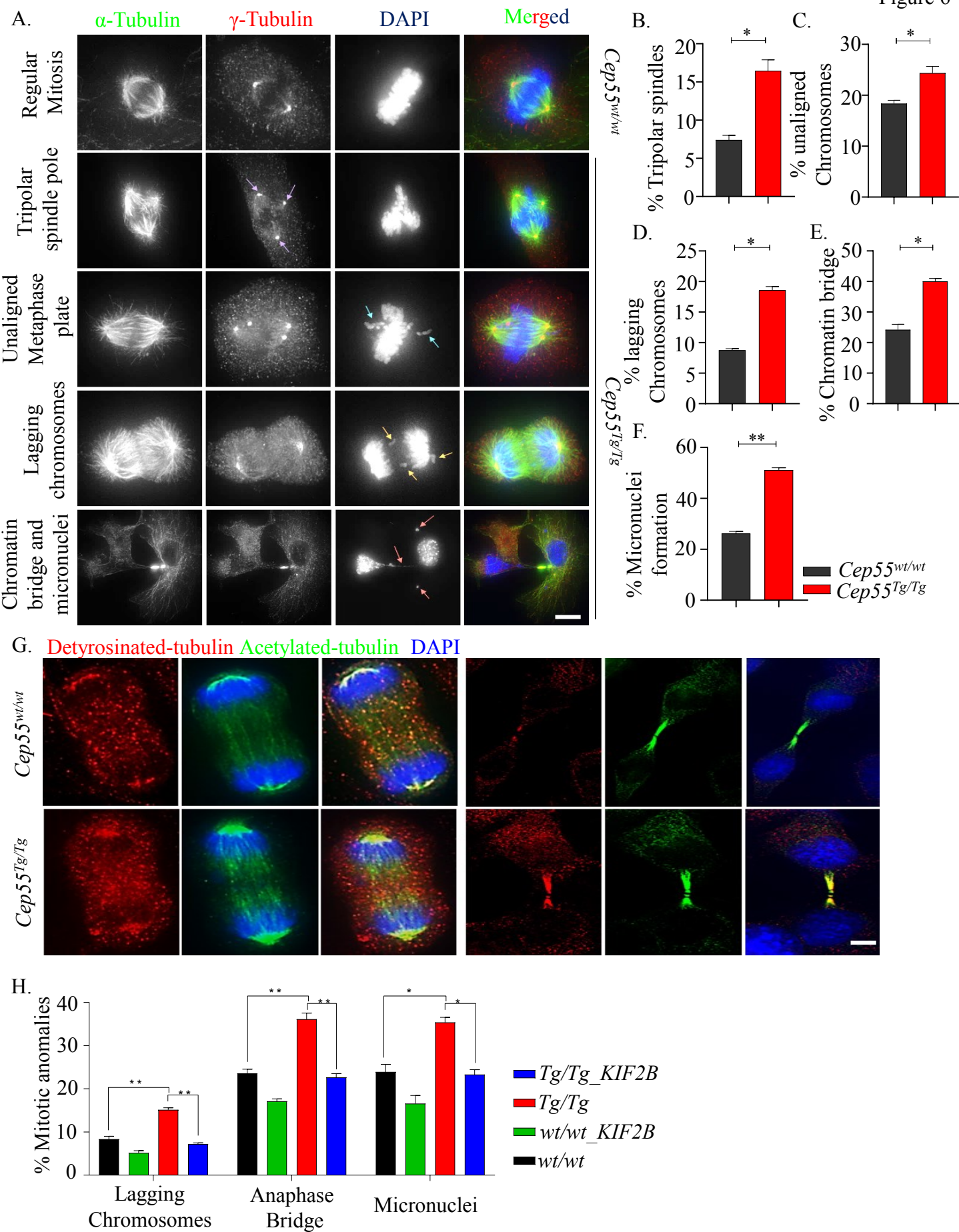| No.	Cancerous Lesions	$Cep55^{wt/wt}$ (n=40)		$Cep55^{wt/Tg}$ (n=40)		$Cep55^{Tg/Tg}$ (n=50)		$Cep55^{wt/wt}$ vs $Cep55^{Tg/Tg}$, $Cep55^{wt/Tg}$ vs $Cep55^{Tg/Tg}$	
		#	%	#	%	#	%	*p* values[a]	
1	Lymphoma	0	0	0	0	18	51.42	6.0×10^{-6}	6.0×10^{-6}
	B-Cell Lymphoma	-		-		11	61.11	0.0010	0.0010
	T-Cell Lymphoma	-		-		7	38.88	0.0159	0.0159
2	Sarcoma	0	0	0	0	9	25.71	0.0039	0.0039
	Fibrosarcoma	-		-		3	33.33	0.2509	0.2509
	Hemangiosarcoma	-		-		6	66.67	0.0317	0.0317
3	Lung (pulmonary) adenocarcinoma	0	0	0	0	6	17.14	0.0317	0.0317
4	Hepatocellular Carcinoma	0	0	0	0	3	8.57	0.2509	0.2509
5	Gastric Carcinoma	0	0	0	0	5	14.28	0.0632	0.0632
6	Intestinal Papillary Carcinoma	0	0	0	0	3	8.57	0.2509	0.2509
7	Myelogenous Leukemia	0	0	0	0	7	20	0.0159	0.0159
8	Hyperplasia	1	2.22	4	8.69	12	34.28	0.0051	0.1019
9	Follicular Hyperplasia	1	2.22	4	8.69	8	66.66	0.0398	0.5373
10	Endometrial Hyperplasia	0	0	0	0	4	33.33	0.1259	0.1259
11	Lipoma	0	0	0	0	1	2.9	1.0	1.0
12	Alveolar-Bronchiolar Lung Adenoma	0	0	10	22.22	15	42.85	0.0001	0.6426
13	Hepatoma	0	0	2	4.34	2	5.7	0.5006	1.0

[a]*P* values: Fisher's exact tests.

Table 2: Changes in chromosomal alterations in *Cep55* transgenic MEFs.

Genotype	Karyotype	Phenotype
Cep55^{wt/wt}	77,XXXX,-6,-7,-18[17]	Hypotetraploid with numerical abnormalities.
Cep55^{wt/Tg}	80,XXXX[6]/77,idem,-6,-7,-18[11]/40,XX[4]	Four normal female metaphases. Six tetraploid metaphases and eleven hypotetraploid metaphases with the same numerical abnormalities that were seen in the WT cell line.
Cep55^{Tg/Tg}	72~74,X,der(X)t(X;11)(F?1;A?2),i(X)(A1)x2,del(1)(A?E?),del(2)(?B?H),+3,-4,-6,-7,del(8)(A?2),-9,der(9)(9pter->9?F::2??2?F::1?H>1qter)[3],der(9)t(9;17)(F?;E?1)[2],+10,+10,del(10)(A2B4)x3,-11,-12,der(13)(13pter->13?::8?->8?::13?->13?:: 8?->8?:: 13?->13qter)[12],der(13) (13pter->13?::8?->8?::13?->13?:: 8?->8?:: 13?->13qter)[2], der(13) (13pter->13?::8?->8?::13?->13?:: 8?->8?:: 13?->13?::15?-> 5qter)[3],der(13)t(13;14)(A?;B?)[2],-15,dup(15)(ED?2),-17,der(17) t(9;17)(?F1;?B)[3],i(17)(A1),-18,-19[cp17]	Hypotetraploid with complex numerical and structural abnormalities.

Note: ? = questionable identification of chromosome or chromosome structure

Supp. Table 1: Distribution of cancer spectrum in bi-transgenic mice.

No.	Cancerous Lesions	$Cep55^{wt/wt}$ $Trp53^{+/+}$ (n=10) a		$Cep55^{wt/Tg}$ $Trp53^{+/+}$ (n=11) b		p value a - b	$Cep55^{wt/wt}$ $Trp53^{+/-}$ (n=17) c		$Cep55^{wt/Tg}$ $Trp53^{+/-}$ (n=15) d		p value c - d
		#	%	#	%		#	%	#	%	
1	Lymphoma	0		0		n/a	8	70	9	64.28	0.5023
	B-Cell Lymphoma	0		0		n/a	3	37.5	6	66.67	0.2433
	T-Cell Lymphoma	0		0		n/a	5	62.5	3	33.33	0.6911
2	Sarcoma	0		0		n/a	5	50	8	53.33	0.2804
	Fibrosarcoma	0		0		n/a	4	80	5	62.5	0.6989
	Hemangiosarcoma	0		0		n/a	1	20	2	25	0.5887
	Leiomyosarcoma	0		0		n/a	0	0	1	6.67	0.4688
3	Lung Adenocarcinoma	0		0		n/a	0	0	2	14.28	0.2117
4	Gastric Carcinoma	0		0		n/a	0		2	14.28	0.2117
5	Intestinal Carcinoma	0		0		n/a	0		1	6.67	0.4688
6	Myelogenous Leukaemia	0		0		n/a	0		2	14.28	0.2117
7	Alveolar-Bronchiolar Lung Adenoma	0		1	10	1.00	0	0	6	42.85	0.0055
8	Hyperplasia	0	0	2	9.9	0.4762	5	29.4	6	40	0.7120
9	Follicular Hyperplasia	0	0	3	27.3	0.2143	3	70	4	66.7	0.6783
	Endometrial Hyperplasia	0	0	0	0	n/a	2	30	2	33.3	1.00

P values: Fisher's exact tests.